The authors have provided a detailed account of ice particle residue (IPR), hydrometeor, and aerosol measurements at the Jungfraujoch station during the winter of 2013 using single-particle measurements and a series of different inlets. Results show the differentiation in IPR type dependent on cloud and meteorological conditions, and aerosol source, in comparison to the background aerosol composition. The authors found that IPR were generally enriched in organic material at higher temperatures, and partly internally mixed with black carbon. Minerals and lead were also observed to be dominant in the IPR, but at lower temperatures. Although these results provide another useful reference for ice nucleation measurements in the literature, the manuscript suffers from a few issues discussed below. After these issues are addressed, I believe this manuscript is suitable for publication in ACP.

Changes in the manuscript are highlighted as follows:

Referee#1	*→ yellow*
Referee#2	*→ green*
Referee#3	*→ red*
Additional changes	*→ blue*

General concerns:

The new findings are not emphasized or discussed enough. The authors demonstrated that mineral dust serves as ice nuclei (IN), however the finding that OC was found on most of the IPR is interesting and a somewhat novel finding. Could it be that the organic material is biological in origin? This is hinted at in the discussion, but should be emphasized.

It could be that a part of the organic material is of biological origin. Most of the organic material shows C_n-Fragmentation ($n = 1$-3) and the fragmentation of aliphatic hydrocarbons ($C_nH_{2n\pm1}$). In some minor cases we found oxidized organic carbon and nitrogen-containing carbon, which may indicate biogenic origin. However, due to the lack of anion spectra we cannot unambiguously classify those particles as biological particles. It is also possible and more probable (winter time and long range transport), that this organic material results from a coating by secondary organic. Therefore, all particles with an organic pattern are summarized to the OC cluster and are not classified in more detail.

Could they be organic particles that contributed to riming versus ice nucleation? This could most certainly happen during the residue drying process and should be noted.

It is expected that ice particles with a size range of 20 µm and smaller grow only by water vapor diffusion and there is a negligible probability that they scavenge aerosol particles by impaction and riming. Thus, the released residual particles by the Ice-CVI can be interpreted as the original ice nuclei This has been discussed already in the Ice-CVI method paper (Mertes et al., 2007) and is supported by the references cited therein.

Discussing these IPR in more detail in addition to focusing on their sources using HYSPLIT analysis would be beneficial and enable the uniqueness of the results to stand out.
The general region of air mass origin is discussed, however, there seems to be a dearth of discussion on the potential sources of the IPR. What types of possible sources are found in each of the different transport regions, such as Figs 3 and 6.

During the cloud events the air masses arrived at the measurement platform from western direction, from North America over the Atlantic Ocean and France. Therefore, particle composition is influenced by different sources (marine, biological and anthropogenic sources) and aging processes. However, also local emissions like residential heating emissions, diesel/fuel exhaust, cooking emissions, etc., cannot be ruled out because of the large skiing area that is situated in the Swiss Plateau. It is therefore hard to say which source influenced which event mostly because all events have more or less the same air mass origin. Because of the low counting statistics during the cloud events it is not possible to further analyze the chemical composition of the ice particle residuals for their origin.

Page 16 line 27-30

The abstract is essentially a list of results. The authors could revise to provide more context as to why their observations and measurements are important on a boarder scale. For instance, the abstract could be started with a few sentences on the motivation for the study. The remainder of the sentences are predominantly composed of results, but can the authors provide a few sentences on why the findings are important? What do they mean in general? Closing with a more general statement on their importance would help as well.

We extended the abstract according to the reviewer's suggestions. Page 1 line 24-27.

Please define acronyms before using them. Once, defined no need to redefine (i.e., JFJ is defined twice). Also, please define the acronym for the field campaign (i.e., CLACE).

The acronym of CLACE was defined. Page 1 line 28.

Where interstitial aerosols investigated? It has been shown that these types can vary quite drastically from ice residues and clear aerosol. It would be interesting to comment on this if they were indeed measured. If not, please clarify.

No, interstitial aerosol was not investigated. In section 2.1 it is described which types of aerosol with which inlet was measured.

The contribution of residues from rime droplets to the full ice crystals is not discussed. Surely, some if not most of the ice crystals analyzed have been rimed, which is an efficient process in a mixed-phase cloud system. The authors need to address the contribution of rimed species to the original ice nucleus residue.

As stated above and in Mertes et al. (2007), small ice crystals grow by water vapor diffusion until they reach a size of about 50 µm. Thus, the ice crystals sampled by both Ice-CVI and ISI (upper cut-off: 20 µm) have not been subject to riming (see also Kupiszewski et al. (2014)).

Section 2.1 Page 4 line 31 – Page 5 line 2.

Specific comments:

Page 1 line 26: 200-900 nm is referring to IPR after drying, correct? Please confirm in text.

Yes, the size range 200 – 900 nm is referring to IPR after drying. But particularly, this size range holds for all particles measured with the ALABAMA. The sampling efficiency of the ALABAMA is the best in this size range. For better understanding we rearrange this sentence.

Page 1 line 29 – 32

Page 1, line 28: Out of curiosity, how did the clear air temperature compare?

The temperature mentioned in the abstract is the temperature range over the whole campagne. During non-cloud episodes the temperature range was between -6.7 °C and -27.3 °C. There are no differences regarding the temperatures between cloud and non-cloud events.

Page 16 line 10 – 12.

Page 1, line 29: State that "background aerosol" refers to cloud free air aerosol. Were interstitial aerosol measured? Also, reiterate that both composition and size were determined for background aerosol.

During this campaign no interstitial aerosol was measured. We modified the abstract accordingly.

Page 1 line 29 – 32

Page 2, lines 6-9: Instead of providing ranges for some species and averages for other, be consistent with provide either an average with a standard deviation or range for each type.

We provide ranges the IPR to express the range of the measured values that were obtained using the ISI and the Ice-CVI (Figure 8). The value for the background aerosol refers to the whole background aerosol data set as given in Figure 8.

Page 2, lines 17-18: Saying aerosols affect solar and thermal radiation is vague. Perhaps use the term radiation budget, or explain these a little more.

We changed the text accordingly.

Page 2 line 21 – 22.

Page 2, line 28: It would be benefit the authors to explain the Wegener-Bergeron-Findeisen process here, and that the riming of ice crystals from supercooled droplets is what causes enhanced precipitation.

An explanation of the Wegener-Bergeron-Findeisen process was added.

Page 2 line 33 – Page 3 line 7.

Page 3, line 4: What do the authors mean by important? Technically, biological particles are the most efficient, but dust is the most abundant. Please clarify.

It was clarified in the manuscript. Because of its abundance mineral dust is the most important ice nuclei but biological particles the most efficient ice nuclei (Hoose et al., 2010).

Page 3 line 13 – 23.

Page 4, line 16: What temperature was the inlet heated at? Wouldn't there be an issue with low molecular weight organics or nitrate/sulfate evaporating from the residues in the inlet?

The temperature of the total inlet is regulated to 20 °C (Weingartner et al., 1999). Sulfate is unlike to evaporate, but evaporation of nitrate is possible. However, due to technical problems we could not measure anions, therefore we did not detect sulfate and nitrate. It is also possible that volatile organics evaporate from the residues. However, since our analysis is not quantitative in terms of particle mass, and a lot of organic material is detected in the spectra, this effect will only play a minor role, if any.

The temperature was added. Page 4 line 28.

Page 5, line 20: Is this referring to the inlet system of the ALABAMA or the OPC?

The size range from 0.25 to 52 µm refers to the size channel boundaries recorded by the OPC. We rearranged this sentence to make it more clearly.

Page 6 line 3 – 5.

Page 5, lines 17-27: The size ranges defined do not correspond to that of the abstract. Why is only 200-900 nm presented? How can 200 nm be achieved if the lens only measures down to 250 nm? What are the two values for transmission efficiency for?

The ALABAMA covers a size diameter range from approx. 100 – 3000 nm (with best transmission from 200 to 900 nm) and the Sky-OPC from 250 – 52000 nm. This section was rearranged for clarification.

Page 5/6 line 33 – 5 and Page 6 line 11 – 13.

Page 6, line 2: Why are only supercooled droplets >5 um removed?

The traditional CVI downstream of the droplet pre-impactor segregates particles smaller than 5 µm in diameter. Thus, the supercooled droplets < 5 µm are removed from the sample flow by the CVI, so that it is sufficient to use a size cut of > 5 µm for the droplet pre-impactor to exclude all supercooled droplets. This is not explicitly mentioned in the indicated text passage and is now reworded to make this point more clear.

Page 6 line 24 – 32.

Page 6, line 4: How do the ice crystals not stick to the surface of the plates? Does the ice from the supercooled droplets freeze fast enough? Is there any loss of ice crystals to the chilled plate?

The idea of such a droplet pre-impaction for the Ice-CVI design was mainly inspired by the work of Tenberken-Pötzsch et al. (2000). They showed using a cooled impactor with several stages that the drop and ice particle residuals are found on the first and the last stages, respectively. Mertes et al. (2007) did lab tests that showed a 100 % sticking efficiency for supercooled drops on the cooled impaction stages and no significant changes within the *measurement uncertainty in the ice particle concentration before and behind the impactor. The latter is the consequence of low velocities that avoid ice particle shattering (which would otherwise lead to an increase of ice particles) and a readily bounce off of ice particles from ungreased surfaces (which would otherwise lead to a decrease of ice particles), which was also observed by Murphy et al. (2004). Comparison with directly measured ice particle and ice particle residue concentration indicate at least that both are in the same order of magnitude. More detailed information is now given in the respective text passage.*

Page 6 line 24 – 32.

Page 7, line 17: Rename section to "Additional instruments" or "Supplement instruments"

The headline was changed into "Supplement instruments".

Page 7, line 21: Why was 20 chosen as the threshold, and is this unit correct? Shouldn't it be something along the lines of g m^{-3}?

The unit is mg m^{-3}. *The typo was corrected.*

Page 8 line 21.

Page 7, lines 30 and on: No need to introduce SEM if there are no results discussed in the current manuscript.

Results of the ESEM are presented in Figure 10. The size of the collected IPR on impactors is measured by ESEM and compared to the sizes of the IPR analyzed by ALABAMA.

Page 8, line 23: What was the percentage of residues that were classified out of all residues measured?

All measured ice residues were classified. The spectra which could not be classified as one of the seven particle types were sorted into the "others" cluster.

Page 9, lines 22 and on: The BioMinSal type presented here is very similar to the residues observed by Creamean et al. (2013). This is a great finding in that this type has been observed elsewhere. The authors should reference Creamean et al. (2013) and perhaps provide a brief discussion on their similarities.

Creamean et al. (2013) report the finding of dust particles mixed with biological particles. However, the Bio/Min/Sal cluster includes spectra, which show only metal ions. The source of these metals is unclear and can be attributed to dust or biological or salt particles (see explanation in section 2.6). The particles in the cluster are not necessarily (ad even unlikely) a mixture of all three compounds. To make this statement more clear we decided to rename the cluster to Bio/Min/Sal.

Page 10, line 14: Make the title more proactively descriptive, i.e., "Ice particle residue composition and potential aerosol sources".

The section title was changed into "Ice particle residual composition and potential aerosol sources".

Page 10, lines 22-25: The event classification is somewhat vague. More information is needed to differentiate these events. What were the temperature ranges of each? What was the wind direction? Etc?

The Ice-CVI events were classified according to the sample efficiency and properties of the Ice-CVI. Due to closer consideration of the (++)- and (+-)-events and taking into account that the ALABAMA did not measure the whole cloud event at the Ice-CVI we get a new classification with more (++)-events which are now called (++)/(+-)-sampling-periods (Table 1). The average temperature, wind direction and wind speed of each event were added.

Page 12 line 16 – 26.

Page 11, line 3: So, the ISI measures IN and CCN, correct? This is what I gathered from the methods. How do the authors eliminate contribution from CCN/droplets? This should be clarified.

No, the ISI measures ice particle residuals (IPR) obtained after the ice crystals sampled through the inlet are evaporated – it does not measure CCN. Droplets are evaporated within the inlet itself in the droplet evaporation unit, a chamber with ice-coated inner walls. Due to the differences in saturation vapour pressures over ice and water, liquid droplets evaporate in the chamber, while ice crystals are affected to a much lesser degree. The CCN released in this process are subsequently removed together with the interstitial aerosols using a pumped counterflow virtual impactor (PCVI), which separates particles based on their inertia, with only larger (aerodynamic diameter > ca. 5 µm) particles (i.e. the ice crystals) transmitted through the PCVI. As the ISI is composed of a number of components, we refer the reader to Kupiszewski et al. (2014), where the operating principle of the inlet and all the components are described in detail.

Page 11, line 18: What were the initialization parameters for HYSPLIT (starting altitude, times initialized, hours back, etc)? These should be provided in the text.

The initialization parameters were added in the text. The starting altitude was 3580 m asl; initialization time: end of the current event; hours back: 72 h.

Page 13/14 line 30 – 1.

Page 11, lines 18-31: It would be helpful to provide the average temperature or wind direction for the events Fig 3 (or any figures with pie chart comparisons for that matter).

We added average temperature and wind direction and speed of each event in Table 1.

Page 12, line 8: Were the lead artifacts a large percentage of the particles (provide the percentage)?

We assume that particles originating from contamination of mechanical re-suspension of lead containing particles from the surface of the impaction plate produce large homogeneous lead-rich particles. This is explained in detail in the paper by Worringen et al. (2015). Our measurements do not show any spectra containing only lead. Therefore, we assume that the sampled lead containing particles are no artifacts.

Page 14 line 18 – 25.

Page 12, line 15: Why were these events chosen? A sentence or two describing the reasoning for showing these warranted.

The six Ice-CVI-sampling-periods were chosen because of the (++) classification (no secondary ice or snowflakes sampled) and the need for sufficient particle mass spectra.

The ISI event was chosen because only during this event a sufficient number of mass spectra was recorded. This is now explained in the text.

Page 14 line 28 – 31.

Page 13, line 19: Clarify that these are referring to background aerosol measurements.

The CPC measurements were done simultaneously during cloud conditions at the total-inlet. This is now stated clearly in the text.

Page 16 line 2 – 4.

Page 13: More discussion is needed on why the events are so different. Is it due to temperature, wind direction, air mass source, etc.

In section 3.2 we already discussed in detail the possible impact of temperature and air mass origin (source and differences in altitude) on the chemical composition of these seven different events. Further discussion would result in pure speculation and does not seem appropriate here.

Creamean, J. M., Suski, K. J., Rosenfeld, D., Cazorla, A., DeMott, P. J., Sullivan, R. C., White, A. B., Ralph, F. M., Minnis, P., Comstock, J. M., Tomlinson, J. M., and Prather, K. A.: Dust and Biological Aerosols from the Sahara and Asia Influence Precipitation in the Western U.S. , Sciencexpress, 1-10, 2013.
Hoose, C., Kristjánsson, J. E., and Burrows, S. M.: How important is biological ice nucleation in clouds on a global scale?, Environmental Research Letters, 5, 024009, 10.1088/1748-9326/5/2/024009, 2010.
Kupiszewski, P., Weingartner, E., Vochezer, P., Bigi, A., Rosati, B., Gysel, M., Schnaiter, M., and Baltensperger, U.: The Ice Selective Inlet: a novel technique for exclusive extraction of pristine ice crystals in mixed-phase clouds, Atmospheric Measurement Techniques Discussions, 7, 12481-12515, 2014.
Mertes, S., Verheggen, B., Walter, S., Connolly, P., Ebert, M., Schneider, J., Bower, K. N., Cozic, J., Weinbruch, S., Baltensperger, U., and Weingartner, E.: Counterflow Virtual Impactor Based Collection of Small Ice Particles in Mixed-Phase Clouds for the Physico-Chemical Characterization of Tropospheric Ice Nuclei: Sampler Description and First Case Study, Aerosol Science and Technology, 41, 848-864, 2007.
Murphy, D. M., Cziczo, D. J., Hudson, P. K., Thomson, D. S., Wilson, J. C., Kojima, T., and Buseck, P. R.: Particle Generation and Resuspension in Aircraft Inlets when Flying in Clouds, Aerosol Science and Technology, 38, 401-409, 2004.
Tenberken-Pötzsch, B., Schwikowski, M., and Gäggeler, H. W.: A method to sample and separate ice crystals and supercooled cloud droplets in mixed phased clouds for subsequent chemical analysis, Atmospheric Environment, 34, 3629-3633, 2000.

Weingartner, E., Nyeki, S., and Baltensperger, U.: Seasonal and diurnal variation of aerosol size distributions (10<D<750 nm) at a high-alpine site (Jungfraujoch 3580 m asl), Journal of Geophysical Research-Atmospheres, 104, 26809-26820, 1999.

Worringen, A., Kandler, K., Benker, N., Dirsch, T., Mertes, S., Schenk, L., Kästner, U., Frank, F., Nillius, B., Bundke, U., Rose, D., Curtius, J., Kupiszewski, P., Weingartner, E., Vochezer, P., Schneider, J., Schmidt, S., Weinbruch, S., and Ebert, M.: Single-particle characterization of ice-nucleating particles and ice particle residuals sampled by three different techniques, Atmospheric Chemistry and Physics, 15, 4161-4178, 2015.

In-situ single submicron particle composition analysis of ice residuals from mountain-top mixed-phase clouds in Central Europe

S. Schmidt[1], J. Schneider[1], T. Klimach[1], S. Mertes[2], L. P. Schenk[2], J. Curtius[3], P. Kupiszewski[4], E. Hammer[4*], P. Vochezer[5], G. Lloyd[6] M. Ebert[7], K. Kandler[7], S. Weinbruch[7], and S. Borrmann[1,8]

[1]Particle Chemistry Department, Max Planck Institute for Chemistry, 55128 Mainz, Germany

[2]Leibniz Institute for Tropospheric Research, 04318 Leipzig, Germany

[3]Institute for Atmospheric and Environmental Sciences, Goethe-University of Frankfurt am Main, 60438 Frankfurt, Germany

[4]Laboratory of Atmospheric Chemistry, Paul Scherrer Institute, 5232 Villigen, Switzerland

[5]Institute for Meteorology and Climate Research, Karlsruhe Institute of Technology, 76021 Karlsruhe, Germany

[6]School of Earth, Atmospheric & Environmental Science, The University of Manchester, M13 9 PL Manchester, United Kingdom

[7]Environmental Mineralogy, Institute of Applied Geoscience, Technical University Darmstadt, 64287 Darmstadt, Germany

[8]Institute for Atmospheric Physics, Johannes Gutenberg University, 55128 Mainz, Germany

[*]now at: Grolimund + Partner AG – environmental engineering, 3018 Bern, Switzerland

Correspondence to: S. Schmidt (susan.schmidt@mpic.de)

Abstract

Ice nucleating particles have a high impact on ice crystal formation in clouds and thereby on precipitation and the global radiation budget. Because the chemical composition of these particles plays an important role at the nucleating processes, investigation of the chemical composition of ice nucleating particles is a topic of current research. This paper presents results from the "INUIT/CLACE 2013" (Cloud and Aerosol Characterization Experiment) field campaign at the high alpine research station Jungfraujoch in January/February 2013. The chemical composition of ice particle residuals (IPR) was measured in orographic, convective and non-convective clouds. The submicron particles were analyzed by a single particle mass spectrometer (ALABAMA) under ambient conditions characterized by temperatures between -28 °C and -4 °C and wind speed from 0.1 m s^{-1} to 21 m s^{-1}. Additionally, background aerosol particles in cloud free air were investigated. The IPR were sampled from mixed-phase clouds with two inlets which selectively extract small ice crystals in-cloud, namely the Counterflow Virtual Impactor (Ice-CVI) and the Ice Selective Inlet (ISI). The IPR as well as the aerosol particles were classified into seven different particle types: (1) black carbon, (2) organic carbon, (3) black carbon internally mixed with organic carbon, (4) minerals, (5) one particle group (termed "Bio/Min/Sal") that may contain biological particles, minerals, or salts, (6) industrial metals, and (7) lead containing particles. For any sampled particle population it was determined by means of single particle mass spectrometer how many of the analyzed particles belonged to each of these categories. Accordingly, about 30 % of the IPR and roughly 43 % of the background particles contained organic carbon. The measured fractions of minerals in the IPR composition varied from 10 % to 14 %, while the values for the "Bio/Min/Sal" group were between 20 % and 54 %. Two percent to 20 % of the IPR contained organic carbon mixed with black carbon. Both inlets delivered similar results of the chemical composition and of the particle size distribution, although lead was found only in the IPR sampled by the Ice-CVI. The results show that the ice particle residual composition varies substantially between different cloud events, which indicates the influence of different meteorological conditions, such as origin of the air masses, temperature and wind speed.

1 Introduction

Ice formation in clouds influences the life-time of clouds, the formation of precipitation, and the Earth's solar and thermal radiation budget (Lohmann and Feichter, 2005). There are two major pathways by which ice is formed in the atmosphere: homogeneous and heterogeneous freezing. The spontaneous formation of ice inside droplets at temperatures of lower -37 °C and without any catalysts is called homogenous freezing (Cantrell and Heymsfield, 2005) and occurs in high clouds at a saturation similar to that of liquid water (Koop et al., 2000). Heterogeneous freezing needs particulate catalysts to initiate freezing at temperatures higher than -37 °C in mixed-phase clouds. These catalysts are called ice nucleating particles (INP). There are four different heterogeneous ice formation modes (Pruppacher and Klett, 2010): deposition nucleation, condensation freezing, immersion freezing and contact freezing. Because heterogeneous freezing starts at higher temperatures than homogeneous freezing, ice crystals, which are formed by ice nucleating particles grow faster (by diffusion) and perhaps precipitate first (DeMott et al., 1998). Another reason for faster formation of precipitation is the Wegener-Bergeron-Findeisen process, which plays an important role on cloud formation and precipitation, especially in mixed-phase clouds. In mixed-phase clouds, where supercooled droplets and ice crystals exist, the supercooled droplets evaporate and the water vapor freezes on the ice crystals. Because of the lower saturation vapor pressure over ice than over water the ice crystals will grow at the expense of cloud droplets. This results in a quick freezing of the supercooled water cloud. These iced clouds have a shorter lifetime than supercooled water clouds, because the precipitation formation via the ice phase is more efficient than in warm clouds (Lohmann and Feichter, 2005).

Ice formation is very selective because of the low number concentration of particles that can act as INP. Roughly about one in 10^5 atmospheric particles can act as INP (Rogers et al., 1998; DeMott et al., 2010). The ice nucleation is induced at some point on the surface of the nucleating particle and the ice nucleation ability of different types if aerosol particles is usually described either by an ice active-site density approach or by classical nucleation theory involving a contact angle (see e.g. Steinke et al., 2015, and references therein). Several laboratory, field and model studies (DeMott et al., 2003a; DeMott et al., 2003b; Cantrell and Heymsfield, 2005; Kamphus et al., 2010; Hoose et al., 2010; Hartmann et al., 2011; Murray et al., 2011; Hoose and Möhler, 2012; Murray et al., 2012; Atkinson et al., 2013; Diehl et al., 2014) have shown that certain mineral dusts belong to the most important ice nucleators in the atmosphere because of their high abundance. On the other hand, biological particles like bacteria, pollen and spores (e.g. Diehl et al., 2001; von Blohn et al., 2005; Möhler et al., 2007; Pratt et al., 2009; Prenni et al., 2009; Diehl and Wurzler, 2010) are the most efficient ice nuclei (Hoose et al., 2010). Also soot (e.g. Cozic et al., 2008a; Pratt and Prather, 2010; Pratt et al., 2010) and effloresced salts (Abbatt et al., 2006; Wise et al., 2012) have been found to act as ice nuclei. There is also some evidence that glassy organics (Froyd et al., 2010; Murray et al., 2010), porous particles (Adler et al., 2013) and lead-containing particles (Cziczo et al., 2009; Ebert et al., 2011) have favorable ice nucleation qualities.

Direct measurements of the chemical composition of single INP or IPR (Ice particle residuals = particles remaining after the ice of cloud ice particles is evaporated) are important to better understand ice formation in mixed-phase clouds, to improve the prediction of precipitation, and to evaluate the influence of anthropogenic aerosol on these processes. Measurements of INP/IPR require instrumentation that can separate the INP/IPR from the background or interstitial aerosol particles and supercooled drops and measure the chemical composition online. In several field studies a combination of a CFDC (Continuous Flow Diffusion Chamber;

Chen et al., 1998), a CVI (Counterflow Virtual Impactor; Cziczo et al., 2003; Mertes et al., 2007) which separates the ice crystals from background aerosol and a Single Particle Mass Spectrometer (SPMS; DeMott et al., 2003a; Cziczo et al., 2003; Cziczo et al., 2004a; Cziczo et al., 2004b; Pratt et al., 2009; Corbin et al., 2012) to measure ice nucleating particles were deployed. Previous measurements of INP and IPR (on-line and off-line) conducted at the Jungfraujoch showed that particles consisting of mineral components dominate the ice particles number (Kamphus et al., 2010), but also particles containing black carbon (Mertes et al., 2007; Cozic et al., 2008a) and lead (Cziczo et al., 2009; Ebert et al., 2011) were found to be enriched in IPR.

Here we report on measurements conducted with the single particle instrument ALABAMA (Aircraft-based Laser Ablation Aerosol Mass Spectrometer; Brands et al., 2011) to analyze the chemical composition of IPR sampled by two unique different ice sampling inlets. The goal of these measurements was to investigate the chemical composition of IPR in ambient mixed-phase clouds in upward transported boundary layer air and free tropospheric air at the high-alpine research station Jungfraujoch (JFJ; 3580 m asl) in Central Europe. Additionally, background aerosol was measured by the use of a total inlet during cloud free conditions.

2 Experimental

2.1 Measurement location and meteorological conditions

The intensive field campaign INUIT-JFJ/CLACE 2013 in January/February 2013 at the High Alpine Research Station Jungfraujoch (~~JFJ~~, Swiss Alps; Sphinx Laboratory, 3580 m asl; 7°59’2’’E, 46°32’53’’N) took place in the framework of the DFG (Deutsche Forschungsgemeinschaft)-funded research unit INUIT (Ice Nuclei research UnIT) and the Swiss National Science Foundation-funded *Interaction of aerosols with Clouds and Radiation project* (see also overview paper by Schneider et al., this issue). The IPR were sampled out of mixed-phase clouds by the Ice-CVI (Ice Counterflow Virtual Impactor; Mertes et al., 2007) and the ISI (Ice Selective Inlet; Kupiszewski et al., 2014) and fed into the ALABAMA single particle mass spectrometer (Brands et al., 2011). During cloud free times the ALABAMA was connected to the heated total inlet (20 °C; Weingartner et al., 1999) to sample the background aerosol particles. The Ice-CVI and the total inlet were located in a central position on the roof of the Sphinx Laboratory and the ISI was located at the railing at the eastern edge of the roof. A short description of the instruments is given in Sections 2.2 to 2.5. Both the Ice-CVI and ISI sample only ice crystals smaller than 20 µm. Such small ice crystals have grown only by water vapor diffusion and have an age of less than about 20 seconds (Fukuta and Takahashi, 1999). It is therefore very likely that these ice crystals have formed in the vicinity of the inlets and that the IPR extracted from such fresh ice crystals corresponds to the original IPN. The meteorological conditions during the campaign along with basic information on the encountered cloud types are summarized in Table 1.

2.2 ALABAMA (Aircraft-based Laser Ablation Aerosol MAss spectrometer)

The ALABAMA (Brands et al., 2011) consist of three sections: aerosol inlet, sizing region and desorption/ionization region. The aerosol inlet is an aerodynamic lens (Liu-type; Liu et al., 1995b; Liu et al., 1995a; Liu et al., 2007; Kamphus et al., 2008) which focuses aerosol particles to a narrow beam by utilizing 6 apertures with decreasing diameter. The particles are separated from ambient air and accelerated to 50 – 100 m s^{-1}, while entering the vacuum-system. For optimal sampling conditions the pressure in front of the aerodynamic lens should be between 0.5 hPa and 5 hPa. For this, a critical orifice is used, which limits the flow to 80 cm^3/min under standard working conditions and which reduces the pre-pressure of the lens to 3.8 hPa. During this campaign, the critical orifice was constructed by a constricted O-ring such that also under Jungfraujoch conditions (ambient pressure around 630 hPa) the lens pressure was regulated to best operating conditions. A skimmer separates the first and the second pumping stages. Two continuous wave detection lasers, which are orthogonal to the particle beam, are located in the second pumping stage. As a modification of the instrument described in Brands et al. (2011), two UV laser diodes (Blu-Ray laser; InGaN, 405 nm) are now used. The particles pass through the laser beams and the scattered light is reflected by an elliptical mirror and detected by a photomultiplier tube (PMT). The vacuum aerodynamic particle size (DeCarlo et al., 2004) can be determined from the velocity of the particles by calibration with particles of known size. In this section the ablation laser (pulsed Nd-YAG-Laser, 266 nm; 6 – 8 mJ per pulse, 5.2 ns per pulse, max. 21 Hz) is triggered. If one particle passes through both laser beams, the in-house designed and built electronic control system sends out a trigger signal to the ablation laser, the laser shoots and ionizes the particles. The ions are separated in the Z-shaped bipolar time-of-flight mass spectrometer (TOFWERK AG, Switzerland) by their mass-to-charge ratio. In principle both signals (for positive and negative ions) can be detected using a multichannel plate (MCP). However, for this study only positive ions were available due to technical issues. The average mass resolution $m/\Delta m$ of the Z-ToF mass spectrometer ranges between 100 for low m/z values and 200 for larger ions (Brands et al., 2011). The ALABAMA covers a size diameter range from 100 to 3000 nm (see Fig. 10) with the most efficient size diameter range being between 200 nm and 900 nm. Particles in the size diameter range of approximately 400 nm were ionized at best.

Additionally the particle size distribution was measured by a Sky-OPC (Optical Particle Counter; Grimm 1.129) with size diameter range from 0.25 to 52 µm. The Sky-OPC is integrated into the ALABAMA instrument upstream of the aerodynamic lens. Due to the size limitation by the inlet system a maximum particle size of approximately 3 µm was measured. Both instruments sampled through ¼’’ stainless steel tubes with different lengths (ISI = 370 cm; Ice-CVI = 126 cm; total = 261 cm). Particle losses inside the sampling tube were calculated with the Particle Loss Calculator (von der Weiden et al., 2009). In the size range between 200 nm and 500 nm the transmission efficiency is about 99 % for all three inlets. The larger the particles and the longer the tubes, the higher are the losses inside the tubes. For a size of 3 µm the transmission efficiency is between 90 % (tube to the Ice-CVI with a length of 126 cm) and 45 % (tube to the ISI with a length of 370 cm). The switching between the three different inlets was performed manually.

2.3 Ice-CVI (Ice Counterflow Virtual Impactor)

The Ice-CVI is designed to sample IPR from mixed-phase clouds. A detailed description and instrumental characterization is provided in Mertes et al. (2007) thus it is only briefly described here. The Ice-CVI uses an omnidirectional inlet, which removes particles larger than 20 µm from the aspired air. The separation of the particles larger than 20 µm out of the sample flow is done with a virtual impactor (VI) downstream of the inlet. After that the supercooled droplets (> 5 µm) are removed by a pre-impactor (PI). The PI consists of impaction plates colder than 0 °C. The supercooled droplets freeze on these plates upon contact while the ice crystals bounce off and remain in the sample flow. Subsequently, a counterflow virtual impactor (CVI, Mertes et al., 2005) rejects interstitial aerosol particles, and potentially remaining supercooled drops and ice particles smaller than 5 µm. Thus, all supercooled drops are pre-segregated by the cut-off behavior of PI and CVI and only small ice crystals, i.e. those with aerodynamic size diameters between 5 µm and 20 µm (cut-off properties of VI and CVI) remain in the sample flow. A transmission efficiency of the PI concerning supercooled drops and ice particles of about 0 % and 100 %, respectively, as expected from Tenberken-Pötzsch et al. (2000) and Murphy et al. (2004), was shown by Mertes et al. (2007).

For complete sublimation, the small ice particles are injected into particle-free and dry carrier air inside the CVI. The aerosol particles that remain after evaporation/sublimation of the ice are termed IPR. The walls of the evaporation tube as well as the carrier air are at room temperature. The IPR can be transferred to different aerosol instruments for physico-chemical characterization. The sampling principle of the CVI leads to an enrichment of the collected particles. This enrichment (factors between 5 and 10) is given by the ratio of the velocity upstream and downstream the CVI inlet tip.

A CPC (Condensation Particle Counter, model 3010, TSI Inc.) was connected downstream of the Ice-CVI at a suitable position for measuring to determine the total particle number concentration of the IPR. Significant non-zero particle number concentrations indicate the presence of ice particles in mixed-phase clouds.

2.4 ISI (Ice Selective Inlet)

Extracting IPR from mixed-phase clouds was also possible with the ISI (detailed description in Kupiszewski et al., 2014). Small ice crystals (the IPR within are assumed to be representative of the original ice nuclei) are segregated from larger ice crystals, supercooled droplets and interstitial aerosol particles by a combination of four inlet components. The first component is the omnidirectional inlet, which is shielded from above in order to prevent large precipitating particles entering the inlet. Subsequently, a custom-made cyclone (BGI Inc.) removes ice crystals, with aerodynamic diameters of ca. 20 µm (D_{50} cut size, i.e., the particle diameter at which 50 % of incoming particles are removed from the sample flow) and larger. Further downstream the removal of supercooled droplets takes place in a custom built ice-coated droplet evaporation chamber using the Wegener-Bergeron-Findeisen (WBF) process. The WBF process is used by deploying a chamber with ice-coated inner walls within the ISI, thus providing an environment in which there is saturation with respect to ice. This in turn means that there is sub-saturation with respect to water (due to the difference in saturation vapour pressures over water and ice), which leads to evaporation of liquid droplets inside the chamber and transfer of water vapour from the droplets to the ice-coated walls of the chamber. The design of the chamber is described in detail in Sect. 2.2 of Kupiszewski et al. (2014). The key difference to the Ice-CVI is that here the separation of supercooled droplets from ice crystals is conducted in the airborne state via evaporation. Finally, the interstitial aerosol and the cloud condensation nuclei (CCN) released during droplet evaporation are removed by a pumped counterflow virtual impactor ($D_{50} \approx 5$ µm). The extracted ice crystals with aerodynamic diameter between 5 µm and 20 µm are heated and the released IPR are transferred into the laboratory for physical and chemical characterization using state of the art single particle aerosol instrumentation (single particle soot photometer (SP2), ALABAMA single particle mass spectrometer, Wideband Integrated Bioaerosol Sensor (WIBS) and a Grimm optical particle counter). The ISI additionally allows for simultaneous counting, sizing and imaging of the hydrometers contained in the cloud with the use of two WELAS (white light aerosol spectrometer; Heim et al., 2008; Rosati et al., 2015) aerosol sensor system (Palas GmbH) and a Particle Phase Discriminator (PPD; Kaye et al., 2008; Vochezer et al., 2015). These are placed behind the cyclone (first WELAS OPSS) as well as behind the droplet evaporation unit (second WELAS OPSS and PPD). The ISI, together with the downstream aerosol instrumentation, thus provides number size distribution of sampled hydrometers and aerosol particles, information on ice crystal shape and surface roughness, as well as number size distribution and chemical composition of ice residual particles.

The ISI enriches the collected particles inside the pumped counterflow virtual impactor with an enrichment factor between 1 and 10.

2.5 Supplement instruments

Particle Volume Monitor (PVM; Gerber, 1996): The PVM measured the liquid water content (LWC = total liquid water present in a cloud) and the surface area of cloud droplets (e.g., Wendisch, 1998). Cloud droplets cross a laser beam and the scattered light is measured. Elevated LWC values are used to identify cloud events, using a threshold value of 20 mg m^{-3}. During the measurement campaign two PVMs were operated by PSI (Paul Scherrer Institute) and the University of Manchester.

Cloud Droplet Probe (CDP): The CDP is a forward-scattering spectrometer for determination of particles sizes and concentrations of cloud droplets. Counting and sizing of the particles is done by detecting light scattered by the particles (for more details see for example Lance et al., 2010).

Scanning electron microscopy (SEM): Ice particle residuals (IPR) were collected by a two stage impactor system (50 % cut-off aerodynamic diameters 1.0 and 0.1 µm, respectively) on transmission electron microscopy grids and elemental boron substrates and analyzed by scanning electron microscopy (SEM, FEI Quanta 200 FEG, FEI Eindhoven, the Netherlands) and energy-dispersive X-ray fluorescence (EDX, EDAX, Tilburg, The Netherlands) to characterize the particles with regard to their chemical composition, morphology, size, internal mixing state and electron beam stability (volatility). (For further details see Kandler et al., 2011). Here we only present the size distribution of IPR measured by SEM and compare them to the IPR sizes obtained by the ALABAMA and the Sky-OPC. Detailed results on the chemical composition analysis of IPR, INP, and background aerosol by SEM are given in Worringen et al., 2015.

2.6 ALABAMA data evaluation

The data evaluation was done with the software package CRISP (Concise Retrieval of Information from Single Particles; Klimach, 2012) based on the software IGOR Pro (Version 6, WaveMetrics) and following the procedure described in Roth (2014). This software package includes mass calibration, conversion of the mass spectra into ‘stick’ spectra by integration over the peak width, and various procedures to sort the mass spectra into groups or clusters of similar spectra. This sorting can be done manually, by means of cluster algorithms (*fuzzy c-means* or *k-means*), or by searching for certain parameters (e.g., ion signals at a certain m/z ratio).

The Clustering depends to some degree on the interstitial settings of the algorithm and its parameters. The start parameters are *Normalization type and time*, *Preprocessing type*, *Initialisation type*, the *number of clusters* and the *start cluster difference.* Using the *fuzzy c-means* algorithm (e.g. Bezdek et al., 1984; Hinz et al., 1999; Huang et al., 2013) the parameters *fuzzifier* and *fuzzy abort* have to be set accordingly. The cluster parameters are explained in detail in the appendix.

As only the cations were detected during the INUIT-JFJ/CLACE 2013 campaign the grouping of the clusters into different particle types by using certain marker peaks was difficult in some cases. At the end, seven different particles types were extracted: black carbon (BC), organic carbon (OC), internal mixture of black carbon and organic carbon (BC/OC), lead containing particles, industrial metals, Bio/Min/Sal (containing possibly bioparticles, minerals or salts), and minerals. The average mass spectra of each particle type are shown in Figure 1. The association of the mass spectra to the individual particle types is explained in detail below. The error limits of the number of mass spectra per particle types was estimated using counting statistics.

Organic fraction: Black carbon (BC) and organic carbon (OC)

The clusters categorized as BC are due to the presence of the typical fragmentation of C_n^+ (Dall'Osto et al., 2004; Pratt and Prather, 2010) of higher mass-to-charge ratios (see Fig. 1a). In comparison to the black carbon, the organic carbon cluster (Fig. 1b) shows different fragmentations of aromatics ($[C_4H_3]^+$ (m/z 51); $[C_5H_3]^+$ (m/z 63); $[C_6H_5]^+$ (m/z 77); $[C_7H_7]^+$ (m/z 91) (Dall'Osto and Harrison, 2006; Pratt and Prather, 2010)), amines ($[CHN]^+$ (m/z 27); $[C_3H_8N]^+$ (m/z 58) (Pratt and Prather, 2010)) or other organic material ($[C_2H_3]^+$ (m/z 27); $[C_3H]^+$ (m/z 37); $[CH_3O/CHNO]^+$ (m/z 43); $[C_4H_2/C_3N]^+$ (m/z 50); $[C_3H_7O]^+$ (m/z 59); $[C_{11}H_{10}/C_8H_{16}NO]^+$ (m/z 142) (Pratt and Prather, 2010)). Black carbon internally mixed with organic (BC/OC) shows both fragmentation types of $[C_n]^+$and $[C_nH_mNO]^+$ (Corbin et al., 2012; Fig. 1c).

Closer consideration of the three different carbon clusters (BC, BC/OC, OC) shows that potassium is present in nearly every mass spectrum in the background aerosol. In the background aerosol 45282 mass spectra including black or organic carbon were measured: 92 % of all these mass spectra show potassium. The BC-type includes the mass spectra without potassium (20 %; only 1 % in the OC/BC-type and 6 % in the OC-type). The same observation holds for the IPR composition measured using the Ice-CVI (Section 3.1): The particle types including organic carbon show more spectra including potassium (91 % of all OC and OC/BC). In contrast to that the particle type including organic carbon measured while using the ISI show more spectra without a high potassium peak (77 %). Previous investigations show that the presence of high potassium peak in the mass spectra in combination with organic carbon is a marker for biomass burning (e.g. Pratt and Prather, 2010; Twohy et al., 2010; Corbin et al., 2012) or biogenic aerosol (e.g. Trimborn et al., 2002; Pratt and Prather, 2010). However, because only cations were measured during this experiment, spectra with a potassium peak mixed with BC and OC cannot clearly assigned to biomass burning or biological particles.

Lead containing particles

Previous measurements at the Jungfraujoch showed that lead-containing particles can be found in IPR (Cziczo et al., 2009; Ebert et al., 2011). The cluster of lead containing particles shows the typical isotope pattern of lead (m/z 208, 207, 206, 204; Fig. 1d).

Industrial metals

The cluster classified as ‘industrial metals’ (Fig. 1e) shows metal signals from anthropogenic (urban/industrial) emissions like $[Cr]^+$ (m/z 52, 53, 54, 50), $[Co]^+$ (m/z 59), $[V]/[VO]^+$ (m/z

51/67), $[Fe]^+$ (m/z 54, 56), $[Mn]^+$ (m/z 55), $[Ni]^+$ (m/z 58, 60, 61, 62) and $[Zn]^+$ (m/z 64, 66, 68) (de Foy et al., 2012). Chromium and nickel containing particles might also be due to contamination from stainless steel tubes. However, due to the low flow speed and laminar flow conditions in our sampling tubes we can exclude abrasion of material by collision of aerosol particles with the flow tube walls. Possible sources for steal contaminations particles are only opening and closing of the valves. Thus, detection of such “industrial metals” particles within a few seconds after opening/closing of a valve indicates contamination artifacts. However, during these time periods no particles of the type “industrial metals” were detected and therefore no particles were excluded as contamination.

Bio/Min/Sal cluster

The spectra in this cluster type contain only metal cations and can therefore not be unambiguously be assigned to a certain particle type. The spectra in the *Bio/Min/Sal* cluster show a mixture or single signals of $[Na]^+$ (m/z 23), $[Al]^+$ (m/z 27), $[K]^+$ (m/z 39, 40), $[Ca]^+$ (m/z 40) and/or $[Fe]^+$ (m/z 54, 56). An example of an average spectrum of this particle type is shown in Figure 1f.

The interpretation of this particle cluster is difficult. The signals are most likely cations of different kinds of salts (Ka_2SO_4 or KNO_3 are more conceivable than sea salt), minerals or primary biological particles, but without corresponding anion an unambiguously assignment to one particle type is not possible. Previous investigations of biological aerosol have shown that metal signals like $[Na]^+$ (m/z 23), $[K]^+$ (m/z 39) or $[Ca]^+$ (m/z 40) dominate the cation spectra (e.g. Frank et al., 2011; Pratt and Prather, 2010; Fergenson et al., 2004). During laboratory studies with test aerosol we also observed mainly single metal signals of sodium and potassium in biological particles, but as well in mineral dust particles. Also iron (Fe^+ m/z 54, 56), which is a typical marker for mineral dust, was observed to occur in some biological particles (maybe due to hemoglobin or due to other ions with an m/z of 56). For these reasons the cluster “Bio/Min/Sal” cannot be further differentiated in this study.

Minerals

Typically marker peaks of minerals are: $[Li]^+$ (m/z 6, 7), $[Mg]^+$ (m/z 24, 25), $[Al]^+$ (m/z 27), $[Si]/[SiO]^+$ (m/z 28, 29, 30/44), $[Ca]^+$ (m/z 40), $[Ti]/[TiO]^+$ (m/z 48, 46, 47, 49, 50/64) and/or $[Fe]^+$ (m/z 54, 56) (Trimborn et al., 2002; Dall'Osto et al., 2004; Dall’Osto et al., 2010) Clusters containing at least three of the above marker peaks were classified as *minerals* (Fig. 1g).

Others

The cluster *others* includes all particle mass spectra, which are very noisy or could not be unambiguously assigned to any of the above cluster types.

3 Results and Discussion

During the INUIT-JFJ/CLACE 2013 campaign we measured 71064 background aerosol particles during a measurement time of 217 h and 1803 ice particle residuals during a measurement time of 342 h: 1659 spectra behind the Ice-CVI during 273 h and 144 spectra behind the ISI during 69 h.

3.1 Ice particle residual composition and potential aerosol sources

The ALABAMA was used to analyze ice crystals extracted from mixed-phase clouds by two different inlets: ISI and Ice-CVI. The times during which cloud particles were sampled by the ISI were identified using the cloud liquid water content (LWC)-data measured with two PVM instruments (PSI and University of Manchester) and a CDP (University of Manchester) while the times when the Ice-CVI sampled cloud particles were identified using the ice residual concentration measured with the CPC behind the Ice-CVI. According to the Ice-CVI sampling capability, which is described in section 2.3, the cloud event periods where the ALABAMA was coupled to the Ice-CVI were classified. This classification resulted in (++)-sampling-periods, when there was hardly any precipitation or blown snow, so that small secondary ice particles created by crystal-crystal collisions can be neglected and thus INP containing primary ice particles are sampled. For (+-)-sampling-periods, the sampling of small secondary ice particles, that do not contain a particle that served as INP, cannot be excluded, since precipitation and blown snow occurred. As a consequence, the ice particle residues analyzed during (++)-sampling-periods are attributed to INP whereas for (+-)-sampling-periods this relation is not that clear and might be only valid for particles that are larger than at least 300 nm. Table 1 shows the identified cloud events along with sampling time, number of acquired mass spectra, sampling-period classification, and weather conditions and cloud type. The meteorological situation during the whole campaign was mainly influenced by low pressure systems with low temperatures.

The occurrence of artifacts during the measurements using the Ice-CVI as well as the ISI is described in Worringen et al. (2015). Aluminum oxide is an artifact of the measurements with the Ice-CVI and silicon oxide is an artifact of the measurements with the ISI. The impaction plates of the Ice-CVI contain aluminum. When the ice crystals bounce on the impaction plates of the Ice-CVI, some aluminum oxide particles are removed from these plates and can be carried with the air stream to the analysis instrument. The ISI was calibrated with silicon oxide particles, which are remained in the system and occurred during the measurements as artifacts. In our dataset it is difficult to distinguish between artifacts and a real component of a particle. Therefore the peaks of m/z 27 (Al^+) and m/z 43 (AlO^+) with respect of the Ice-CVI measurements and the peak of m/z 28 (Si^+) with respect to the ISI measurements were ignored.

~~In total, we measured 329 spectra during the (++)-events (61 h measurement time) and 1335 spectra during the (+-)-events (160 h measurement time) by using the Ice-CVI. Behind the ISI we measured 144 spectra during 35 h measurement time.~~

Figure 2 shows the results of the clustering algorithm for all ice particle residual measurements. The Ice-CVI data were analyzed separately for all (++)-sampling-periods (left pie chart) and for all (+-)-sampling-periods (middle pie chart). The right pie chart shows the results for all ISI measurements. This analysis shows that the metal containing particle groups (Bio/Min/Sal, industrial metals, and minerals) are the dominating fractions in IPR composition measured by using the Ice-CVI during the (+-)-sampling-periods (49 %) and the ISI (66 %). Interestingly, during the (++)-sampling-periods metal containing particles represent only a smaller fraction (40 %). We also detected lead containing particles, but only while sampling through the Ice-CVI (7 % in the (++) cases and 12 % in the (+-) cases). During the (++)-sampling-periods measured behind the Ice-CVI, black carbon internally mixed with organic carbon (20 %) is one of the main fractions. Together with OC (26 %), these two particle types represent 46 % of all IPR. It is worth noting that there are more similarities between the Ice-CVI and ISI during (+-)-sampling-periods than the (++)-sampling-periods. A reason for that can be that the ISI measurements are also influenced by secondary ice or incoming snowflakes. During the (+-)-sampling-periods as well as during the ISI-sampling-periods precipitation occurred. On the other hand, the measurements at the ISI and the Ice-CVI were not done simultaneously, such that ~~also~~ differences in the air mass origin could play a role here.

Backward trajectories were compiled using CRISP (Klimach, 2012) with access to HYSPLIT (Hybrid Single Particle Lagrangian Integrated Trajectory Model, National Oceanic and Atmospheric Administration; Draxler and Rolph, 2012; Rolph, 2014), which was run using GDAS (Global Data Assimilation System) meteorological dataset (starting altitude: 3580 m asl.; hours back: 72 h; initialize time: end of the current event). The geographical origin of the air masses and change of altitude during the transport can be used to infer whether the air masses are influenced by surface emissions or mainly characterized by free tropospheric air and long distance transport. During all measurement episodes (total, Ice-CVI, ISI) the air masses approached the measurement station from slightly different directions (Fig. 3). The air masses during the (++)-sampling-periods came primarily from north-western directions from North America over France, while during the (+-)-sampling-periods the air masses arrived more from the North, over Scandinavia and Germany. The origin of the air masses during the measurements using the ISI are similar to those of the (++)-sampling-periods but with a tendency towards southern directions (Fig. 3). During non-cloud episodes air masses approached the measurement location from all directions.

Previous measurements at the JFJ showed that there is an enrichment of mineral dust and black carbon in IPR composition (Mertes et al., 2007; Cozic et al., 2008b; Kamphus et al., 2010). An enrichment of black carbon is not observed in our measurements. Cziczo et al. (2009) found that lead-containing particles are also enriched in the IPR compared to the background aerosol. Our measurements show also that mineral dust ~~(measured behind the ISI and during the (+-)-sampling-periods)~~ and lead (only measured behind the Ice-CVI) were two of the dominating fractions in the IPR composition. Worringen et al. (2015) report on SEM analyses of particles sampled during the same project behind the ISI and the Ice-CVI. They found lead in two states, namely homogeneous lead-rich particles and small lead inclusions in particles of other material. While the small lead inclusions are not considered as potential artifacts, the large lead-rich particles might be artifacts from mechanical re-suspension of lead containing particles from the surface of the impaction plates of the Ice-CVI. In our case the lead-containing particles are internally mixed with organics, minerals or other metals, therefore we interpret these particles as real atmospheric particles and not as artifacts.

3.2 Event-to-event variability

Figure 4 shows the IPR chemical composition measured during seven different events. These sampling-periods were chosen, because these are (++)-sampling-periods and contamination of e.g. incoming snowflakes are excluded and during these sampling-periods the most particles were measured (except for the ISI measurements). Although the air masses sampled during all seven events have very similar origin and history of altitude (Fig. 5a and 5b) the chemical composition for each event is different from the others. All air masses during these events arrived rising from a western direction to the measurement platform, such that the chemical composition of these seven events was probably influenced by local emissions. During Event 3 and 4 the air masses arrived from a south-western direction. This is reflected in the chemical composition: Both events show organic carbon as the main fraction and the amount of lead containing particles is comparable (13 % Event 3 and 15 % Event 4). The differences between Event 3 and 4 are the absence of BC in Event 4 and of minerals in Event 3. The chemical composition of Event 12 is also comparable to Event 4 and Event 6. In this case also the dominating fractions are OC and Bio/Min/Sal. The absence of lead containing particles (as well as in Event 6) and the presence of 2 % BC/OC in Event 12 or 4 % in Event 6 are the main differences between Event 12, 6 and Event 4.

Another reason for similarities and differences between these 7 events can be the temperature (Fig. 6). Events 3, 4 and 6 have the highest fraction of OC (nearly 50 % of the particles) and Event 6 additionally a high amount of metal containing particles (37 %; industrial metals, minerals and Bio/Min/Sal). Event 3 and 4 have also the highest temperatures (Event 3: average temperature $\bar{T}$ = -7.8 °C; Event 4: $\bar{T}$ = -8.6 °C). In contrast to that, Event 12 has the highest amount of metal containing particles (65 %) and has an average temperature of about $\bar{T}$ = -17 °C. Event 6 has also a high amount of metal containing particles and the lowest average temperature of about $\bar{T}$ = -21 °C. Event 4 has also a high amount (41 %) of ‘metal’ components but by closer consideration of the Bio/Min/Sal-type it can be shown that this type consists mostly of metal ions together with organic ions in Event 4 and more single metal ion signals during Event 12 and 6. This high amount of metal components measured at lower temperatures is also comparable to Event 2 and 5. 62 % of the chemical composition of Event 2 and 51 % of Event 5 consist of metal components. Therefore the data indicate that organic material dominates the IPR composition at higher temperatures and metal components from mineral or salty origin dominate at lower temperatures. This finding is surprising, because previous studies found that organics are ice active only at temperatures below -40 °C (Hoose and Möhler, 2012). However, the organic signal in the mass spectra might also originate from bioparticles, which would explain the ice formation at higher temperatures, because bioparticles have been reported in the literature by many authors to be ice active at higher temperatures (e.g. Möhler et al., 2008; Hoose and Möhler, 2012). Another source can be soil organic matter. Tobo et al. (2014) shows that organic-rich particles are more important than mineral particles for the ice-nucleating ability of agricultural soil dust at temperatures higher than -36 °C. An exception is Event 1. During this event the second lowest temperatures ($\bar{T}$ = -19.2 °C) of all events prevailed, but a high relative amount of organic components was measured (80 % BC/OC and OC). A reason for this high relative amount of organic material can be local emissions. At this time the total particle concentration (measured inside the cloud using the total inlet) shows a short period with high concentrations (> 2000 cm^{-3}, see Fig. 7), which indicates local emissions.

3.3 Comparison between background aerosol particle composition and IPR

During non-cloud phases the ALABAMA was connected to the total inlet to measure background aerosol particles. Figure 8 shows the averaged composition of all background aerosol particles along with the IPR composition measured behind the Ice-CVI during the (++)-sampling-periods and behind the ISI. The temperature range during the background aerosol measurements was between -27 °C and -6 °C, which is comparable to the temperature range of the cloud events. In comparison to the IPR composition, the measurements show a high fraction of black carbon (17 %; Fig. 8) and only a minor fraction of BC/OC (4 %). The fraction of the particle type 'BC/OC' in the background aerosol is comparable to that in the IPR sampled by the ISI. However, also the aerosol particles are dominated by the particle types 'organic carbon' (43 %) and 'Bio/Min/Sal' (30 %). ~~Previous high mountain-top measurements at the Storm Peak Laboratory (SPL; 3200 m asl.) in northern Colorado show also organic as the major component in the background aerosol (DeMott et al., 2003a ;Cziczo et al., 2004a).~~ The differences as compared to the IPR compositions are the negligibly small amount (< 0.1 %) of lead-containing particles and the much smaller amount of minerals (about 1 %). This is partly in contrast to other measurements. Previous measurements with the ATOFMS at the Jungfraujoch as well as airborne measurements over North America show 5 and 10 % lead-containing particles in the background aerosol (Murphy et al., 2007) but also only a small amount of mineral dust or fly ash measured at the Storm Peak Laboratory (SPL; 3200 m asl.) in northern Colorado (DeMott et al., 2003a). Data from the SPL show also organic as the major component in the background aerosol (DeMott et al., 2003a ;Cziczo et al., 2004a). A part of the organic material detected in the IPR as well as in the background aerosol may be due to could be local anthropogenic emissions. In the vicinity of the measurement station is a large and popular skiing region. Additionally, cooking emissions, diesel exhaust or residential heating may also play a role.

~~Previous investigations show that the presence of a high potassium peak in the mass spectra in combination with organic carbon is a marker for biomass burning (e.g. Pratt and Prather, 2010; Twohy et al., 2010; Corbin et al., 2012) or biogenic aerosol (e.g. Trimborn, 2002; Pratt and Prather, 2010). Closer consideration of the three different carbon clusters (BC, BC/OC,~~

~~OC) shows that potassium is present in nearly every mass spectrum. In the background aerosol 45282 mass spectra including black or organic carbon were measured: 92 % of all these mass spectra show potassium. The BC-type includes the mass spectra without potassium (20 %; only 1 % in the OC/BC-type and 6 % in the OC-type). The same observation holds for the IPR composition: The particle types including organic carbon measured by the use of the Ice-CVI as well as the ISI show more spectra including potassium (94 % of all OC and OC/BC spectra while using the Ice-CVI and 98 % while using the ISI). Because of this results spectra with a potassium peak cannot clearly assigned to biomass burning or biological particles.~~

3.4 Influence of the air mass trajectories on the aerosol composition

The chemical composition of the background (out-of-cloud) aerosol has been shown in Figure 8. The high variability of the measured IPR might be due to the different aerosol properties when air masses arrive from different geographic origin and/or different altitudes at the Jungfraujoch. Therefore, we investigate here how air masses origin influences the aerosol properties. Because of the saddle position of the JFJ, there are only two possibilities of how the air masses can approach the measurement platform (Fig. 6). Predominantly, the air masses arrive from northwestern direction over the Swiss plateau (wind direction of approx. 315°). Less frequently, the approach was from a southeastern direction from the inner Alps (approx. 135°, via the Aletsch Glacier). According to the direction from which air masses approach the measurement platform, the chemical composition is influenced predominantly by anthropogenic and organic emissions or by mineral dust sources. To assess the influence of origin and the average altitude of the air masses during their transport to the Jungfraujoch, we compare two time periods with aerosol measurements using the total inlet (11.02. and 19.02.2013). The chosen time periods exhibit nearly the same relative humidity, potential wet bulb temperature and temperature (Fig. 6).

Fig. 9 shows the chemical composition of the aerosol particles for both time periods, along with corresponding back-trajectories. The comparison shows that more particles containing BC (internally mixed with ammonium or the Bio/Min/Sal-type) and the Bio/Min/Sal-type are observed in the air masses arriving from a northwestern direction (11.02.2013), while the measurements during the SE-event show more OC containing particles (internally mixed with ammonium or the Bio/Min/Sal-type). The fraction of particles measured containing only potassium and pure organic carbon is very similar for both events.

The air masses not only approached locally from different directions, but also had different long-range origins (see back trajectories Fig. 9). The air masses measured on 19.02.2013 (NW-event) approached from the north over Germany and have remained at approximately the same altitude as the Jungfraujoch during the last 72 hours. Thus, these air masses have been in the free troposphere for at least three days prior to the measurement. The chemical composition of the measured particles is dominated by black carbon internally mixed with ammonium and by the Bio/Min/Sal-type. In contrast to the 19.02.2013, the air masses on 11.02.2013 (SE-event) approached over southern France and the western Po Valley, have been lifted from low altitudes and clearly influenced by the boundary layer. These air masses contain higher amounts of OC containing particles. This shows that the vertical uplifting brings anthropogenic emissions (e.g., from the Po Valley) up to the altitude of the measurement station, while the air masses measured during the NW-event contain a higher amount of sea salt or mineral dust (both contained in the Bio/Min/Sal-type) and aged, processed BC particles.

3.5 Size distribution of IPR and background aerosol

Ice-CVI and ISI both extract small ice particles in the size range from 5 µm to 20 µm from mixed-phase clouds (Mertes et al., 2007; Kupiszewski et al., 2014) while the upper cut-off of the total inlet was 40 µm for wind speeds up to 20 m/s (Weingartner et al., 1999). In Figure 10 is shown the size distributions of IPR measured with the ALABAMA (a, c, e) and the Sky-OPC (b, d, f) compared with ESEM measurements (a and b). Figure 10a shows the size distributions of IPR measured by ALABAMA and ESEM applying the Ice-CVI. ~~Figure 10c the size distributions measured by ALABAMA and ESEM using the ISI.~~ In Figure 10b ~~and d~~, the corresponding size distributions measured with the Sky-OPC are shown. Figure 10c shows the size distributions measured by ALABAMA and Fig. 10d measured by the Sky-OPC using the ISI. Fig. 10e and f show the size distribution measured by ALABAMA and the Sky-OPC using the total inlet. The measurement times for Ice-CVI and ISI are given in Table 1; the measurements using the total inlet were done during all cloud-free periods. ~~For all three inlets (total, Ice-CVI, ISI) most of the detected IPR measured with the ALABAMA and also with the Sky-OPC is in the size range of 300 – 650 nm.~~ ~~The IPR size distributions measured by ALABAMA and SEM behind the Ice-CVI are in very good agreement (Fig. 10a). In~~

~~contrast, the IPR size distribution measured behind the ISI are somewhat different. (Fig. 10c): Both distributions show two maxima, but the positions of the maxima are not the same. The ALABMA IPR distribution has a primary maximum in the size bin 0.4 – 0.5 µm and a secondary maximum in the size bin 1.3 – 1.6 µm. The SEM IPR distribution both maxima are shifted to larger sizes. The first maximum is in the 1 – 1.5 µm interval and the second maximum is in the 2 – 2.5 µm interval. However, total count rates are very low, so this difference should not be overemphasized. Furthermore, SEM measured geometric diameters, while the sizes determined by ALABAMA refer to the vacuum aerodynamic diameter.~~ SEM and ALABAMA measure the size distribution in different ways: ALABAMA measures vacuum aerodynamic diameter and SEM geometric diameter. To compare both data sets the SEM data were converted to the aerodynamic diameter. The vacuum aerodynamic diameter was calculated according to DeCarlo et al. (2004) with the assumption that the projected area diameter from the electron microscopy analysis equals the volume-equivalent diameter. Furthermore, an average dynamic shape factor of 1.2 was used for the calculations. This seems to be justified, as most non-extremely shaped particles show low variation in shape factor (Schneider et al., 2006; Zelenyuk et al., 2006), except for soot with high fractal dimension (Slowik et al., 2004) which was not commonly encountered in the present work. The density ratios required for the calculation were estimated from the major composition of the particle according to the values from Weinbruch et al. (2014) (Table S2). The IPR size distributions measured by ALABAMA and SEM behind the Ice-CVI show the same behavior (Fig. 10a) with shifting the SEM graph to larger sizes. Both distributions show a slow increase at small size ranges and a higher number of larger particles. The ALABAMA IPR distribution has a primary maximum in the size bin 300 – 400 µm and a secondary maximum in the size bin 500 – 600 µm. The SEM size distribution shows a single maximum at about 900 µm. However, total count rates are very low, so this difference should not be overemphasized. For all three inlets (total, Ice-CVI, ISI) most of the detected particles measured with the ALABAMA are in the size range of 300 – 800 nm. In contrast to the size distribution measured with the ALABAMA (and also ESEM for the Ice-CVI), the size distributions measured with Sky-OPC (b, d, f) do not show a maximum but only a decreasing number concentration of particles with increasing particle diameter for all three inlet types. The difference to the ALABAMA size distributions is a result of the detection and ionization efficiency of the ALABAMA which is the highest around 400 nm. The IPR size distributions measured with the ESEM and Sky-OPC (10b) show both a decreasing number of particles at larger size ranges. In contrast to the size distribution measured with the Sky-OPC the size distribution measured with ESEM shows a lower number of particles at smaller size ranges. The Sky-OPC size distribution measured behind the ISI (10d) shows an unexplained sudden decrease above 3 µm. Figure 10f shows that the background aerosol particles (Sky-OPC) have a size range of up to approximately 20 µm but with highest number concentration in the smaller range (< 1 µm). The relative amount of larger particles is (d > 1 µm) clearly elevated for the IPR, both behind the ISI and Ice-CVI (10b and d) in comparison to the background particles (10f). Note that the measurements of background particles (out of cloud) and IPR were conducted by definition at different times, such that the absolute amount of particles cannot be compared.

As mentioned above, relatively more IPR larger than 1 µm were observed compared to the background aerosol particles. The percentage of the background aerosol particles larger than 1 µm (vacuum aerodynamic diameter) measured by ALABAMA was only 3 %, while 12 - 13 % of the IPR behind the Ice-CVI and ISI were larger than 1 µm. Therefore, the chemical composition of these particles has been analyzed separately:

Figure 11 shows the chemical composition of the IPR and background aerosol particles larger than 1 µm. The most frequent particle types found in the IPR larger than 1 µm are OC, lead containing particles, Bio/Min/Sal, and minerals for the Ice-CVI, and Bio/Min/Sal and minerals for the ISI. Lead containing particles are found in the IPR sampled by the Ice-CVI to a similar percentage (14 %) as in all IPR (7 %, see Figs. 2 and 8). Interestingly, the background aerosol supermicron particles are dominated by the Bio/Min/Sal-type and OC. The finding strengthens the assumption that the metal ions detected in these mass spectra are likely metal cations of primary aerosol like sea salt, minerals or biological particles, which are mainly found in the coarse mode (e.g., Seinfeld and Pandis, 2006). Such large primary particles are also expected to act efficiently as INP, and it is therefore not surprising that they are found in the supermicrom IPR. More surprising is the large fraction of OC and BC/OC particles detected in the supermicron IPR. These large particles containing organic material appear to be even better INP than the supermicron particles assigned to the Bio/Min/Sal category. It has recently been suggested that porous and glassy organic particles under certain conditions play an important role as INP (Murray et al., 2010; Adler et al., 2013), and this may explain the results presented here. But also the origin of these supermicron organic particles remains unclear. Primary biological material as a source for these particles is regarded to be unlikely, because the marker peaks observed in cations of biological particles (like K^+, $Na^{+,}$ Ca^{2+}) were not observed in these particle spectra assigned to the OC and BC/OC types. However, particle classification of single particle mass spectra is never absolutely certain, and future work may reveal more insight into the nature and origin of these particles.

The particle composition of the particle smaller than 1000 nm closely resembled thr composition of the whole data set, because the particle smaller than 1000 nm dominate the analyzed particles by number. Only the BC/OC-type is increased in the particles smaller than 1000 nm measured while using the Ice-CVI.

~~The size distribution allow also for an estimation of the ice active site (e.g., Vali et al., 2014) density of particles larger than 1 µm compared to those smaller than 1 µm: Assuming that each IPR corresponds to at least one ice active site on the original aerosol particle (otherwise it would not have acted as an INP), we can estimate the ice active site density for the particles analyzed by ALABAMA, separated for particles smaller than 1 µm and larger than 1 µm. The number of ice active sites per IPR surface (ice active site density) is $2.0\cdot10^{-7}$ nm^{-2} for d > 1 µm and $1.6\cdot10^{-6}$ nm^{-2} for particles with d < 1 µm. Relating the number of ice active sites to the total aerosol surface yields $7.1\cdot10^{-10}$ nm^{-2} for d >1 µm and $4.3\cdot10^{-9}$ nm^{-2} for d < 1 µm. In both cases the ice active site density is larger for particles smaller than 1 µm. This is an important finding and explains the high number of IPR found in the size range below 1 µm. However, it should be noted that the assumption that each IPR corresponds to one ice active site may underestimate the number of ice active sites. In cases where more than one ice active site is found on the particles, also only one ice crystal will form and one IPR will remain. Thus the estimated number yields a lower limit for the ice active sites.~~

4 Summary and Conclusions

This paper presents results of the single particle measurements during the INUIT-JFJ/CLACE 2013 campaign conducted at the Jungfraujoch in January/February 2013. In agreement with previous measurements at the Jungfraujoch (Chou et al., 2011; Kamphus et al., 2010; Mertes et al., 2007), it was found that larger particles are more efficient ice nuclei. Specific analysis of ~~only those~~ particles > 1 µm showed that the chemical composition of these larger particles is dominated by organic material and the “Bio/Min/Sal” type, both in the IPR as well as in the background aerosol. Besides, the “minerals” group was found to be one of the main fractions of the IPR measured behind the Ice-CVI. From the finding that IPR have a higher relative number of larger particles than the background aerosol particles we conclude and confirm a better ice nucleation ability for the larger, primary aerosol particles such as minerals, salt and biological particles.

In general, IPR are enriched in organic material, partly also internally mixed with BC. Additionally, minerals and lead were found in IPR as has already been observed in previous measurements conducted at the JFJ (Mertes et al., 2007; Cozic et al., 2008b; Cziczo et al., 2009; Kamphus et al., 2010; Ebert et al., 2011). In comparison to the composition of the IPR measured using the Ice-CVI, the measured composition using the ISI is dominated by minerals, and no lead containing particles were found, while 7 % of the IPR sampled using the Ice-CVI included lead. In contrast to Cozic et al. (2008) we found no enrichment of pure black carbon in the IPR composition. Only the chemical composition of the background aerosol particles shows a high fraction of black carbon. These results agree with previous investigations (DeMott et al., 1999; Dymarska et al., 2006; Hoose and Möhler, 2012) describing black carbon as a good ice nucleus but only at lower temperatures and its ice nucleating ability appears to be reduced if coatings by organic material or sulfuric acid are present. During the INUIT-JFJ/CLACE 2013 campaign the temperatures were never lower than -30 °C; see Fig. 6. In the background aerosol, the main particle fraction is also organic carbon. The high amount of organic material in the background aerosol as well as in the IPR motivates further investigation of different organic material by single particle mass spectrometry to better characterize the organic fraction. While there have been previous observations that organic matter is of general importance for ice nucleation ability (DeMott et al., 2003a; Cziczo et al., 2004b), recent laboratory studies have shown the importance of porous and glassy organic matter for ice nucleation (Murray et al., 2010; Adler et al., 2013).

The investigation of the influence of the temperature and the origin and altitude of the air masses on the chemical composition of IPR and aerosol particles indicate that organic material dominates the IPR composition at higher temperatures and metal components from mineral or salt at lower temperatures which agrees with previous findings (e.g. Möhler et al., 2008; Hoose and Möhler, 2012). It was illustrated that the origin (geographic and altitude) of the air masses influenced the chemical composition of the aerosol particles. For the non-cloud aerosol, the particles sampled in air masses characterized by free tropospheric air and long distance transport were found to be dominated by BC and single metal ions from salt, mineral or biological sources (Bio/Min/Sal-type). These particle types were probably partly mixed with secondary inorganic components, because NH_4^+ was detected in some spectra. In contrast to that, the particles in air masses which are influenced by surface emissions are dominated by organic carbon and potassium.

Appendix A: Parameters underlying the clustering algorithm

This section describes the cluster parameters of the software package CRISP. The chosen parameters are listed in Table A.

Normalization type and time

To compensate for differences in the ionization efficiency, each mass spectrum is normalized to the sum of the signal intensities with preservation of the relative relationship of the signals. By this, the influence of absolute signal intensity is decreased. Absolute signal intensity is not needed because the laser ablation method does not measure quantitatively. The point at which the normalization is applied in the analysis sequence can be chosen. In case of measuring both polarities the spectra of both polarities are first merged, and normalization can be applied before, after or before and after concatenation.

Preprocessing type

Preprocessing (before normalization) can be applied to increase mass signals with lower intensity with respect to signals with a higher intensity, such that the presence of a certain m/z has more significance than the signal intensity in the calculation of the distance to the reference spectrum. Typically the square root of the signal intensities is used.

Initialisation type

This parameter defines the way the reference mass spectra are selected. Two options are available:

- *find different startcluster*: different spectra are randomly selected according to certain criteria
- *random*: reference spectra are chosen randomly

Reference spectra can also be determined manually, however, this last option is not very useful for field data because the number of particle types is unknown.

Number of cluster

The result of the clustering is highly dependent on the pre-selected number of clusters. In the case that the number of clusters is too small, some cluster types cannot be found, while in the case that the number is too large, too many similar spectra are assigned to different clusters. In the fuzzy c-means algorithm all non-matched spectra are collected in a rest cluster.

Cluster difference

This parameter determines the distance between the spectra which are chosen as start references at 'find different startcluster'. The *cluster difference* is between 1 and 0, where a *cluster difference* of 1 means that the chosen startclusters are identically. This distance results from the Pearson correlation and affects the number of the resulting clusters. The number of clusters increases with increasing similarity of the references and is constant at a value of 0.7 (Roth, 2014). If the *cluster difference* is too small, the distinctions between the clusters are too large, resulting in too few cluster types. Thus, it is recommended to use more similar reference mass spectra and to summarize those clusters that show similar mass spectra at the end of the clustering.

Fuzzifier and fuzzy abort

The *fuzzifier* (also called *fuzzy weighting* exponent) is a dimension of fuzziness of the classification of the cluster ($1 \leq fuzzifier \leq \infty$; e.g. Huang et al., 2012). The bigger the *fuzzifier*, the more inaccurate is the assignment to the references, because the spectra cannot exactly be assigned to one cluster. The distance d_{ij} between spectra i and reference j is weighted with:

$$d_{ij}^{\frac{1}{z-1}} \qquad (1)$$

where z is the *fuzzifier*. When the preprocessing option of CRISP is used, it has been found that the result of the clustering is independent of the *fuzzifier* value (Roth, 2014).

During the clustering, each mass spectrum is compared to the reference spectra in terms of distance, membership and correlation. If these parameters fulfill the pre-selected criteria, the mass spectrum is sorted into the cluster represented by the reference and the average spectrum is calculated again. Subsequently all mass spectra are compared again with the reference spectra. This procedure is repeated until the criterion of abort (*fuzzy abort*) is reached, such that the clustering stops when the value of the difference of all reference spectra between two iterations is smaller than the value defined by *fuzzy abort*.

For the data evaluation of the current dataset (both IPR and background aerosol particles) a mixture of manual and automatic clustering was used. First, an automatic clustering was done with the following parameters:

Table A: Chosen clustering parameter.

Preprocessing type	**Power each m/z**
Preprocessing power	0.5
Normalization type	Sum
Cluster difference	0.7 (0.6)
Distance	Correlation
Fuzzifier	1.2
Fuzzy abort	0.0001

As already mentioned the result of the clustering is highly dependent on the chosen initial number of clusters. If this initial number of clusters is too small, some cluster types may not be found. Therefore we chose a high number of clusters. In the case of the background aerosol (71064 spectra) we started the first clustering with 200 clusters. Each of the resulting 200 clusters was manually inspected, and based on its ion signatures it was assigned to one particle type. Those spectra that cannot be sorted by the algorithm into one of the 200 clusters (membership coefficient below a pre-defined threshold) are assigned to a "rest cluster" (12407 spectra in the case of the background aerosol). This rest cluster was clustered again with a reduced condition for the cluster difference and with an initial number of clusters of 25. The number of cluster was still too large after the clustering of the "rest cluster", so it was further analyzed. First, the remaining spectra were sorted by the use of specific marker peaks and the resulting clusters were then clustered again with changing the fuzzyfier from 1.2 to 1.3 and a cluster difference of 0.7. After that, the resulting clusters were manually inspected and sorted (with the criterion $r^2 \geq 0.7$). By this, we could reduce the number of spectra in the rest cluster from 12407 to 3243. Due to this sorting procedure based on both automatic clustering and manual cluster inspection one particle type typically contains different clusters with different fragmentations. For example, the particle type "organic carbon" includes clusters showing aliphatic hydrocarbon, aromatic carbon, nitrogen and oxidized carbon fragmentation patterns. In order to restrict the result to a reasonable number of particle types, we summarized these clusters to one particle type.

Acknowledgements

This work was supported by the DFG projects FOR 1525 (INUIT), SPP 1294 (HALO, grant Me 3524/1-2), the Max Planck Society, the European Union Seventh Framework Programme

(FP7/2007-2013) under grant agreement n° 2662254 (ACTRIS TNA) and the Swiss National Science Foundation (200021L 135356).
The authors gratefully acknowledge the NOAA Air Resources Laboratory (ARL) for the provision of the HYSPLIT transport and dispersion model and/or READY website (http://www.ready.noaa.gov) used in this publication.

We would like to thank Swiss Meteorological Institute (MeteoSwiss) for providing meteorological measurements and the International Foundation High Altitude Research Station Jungfraujoch and Gornergrat (HFSJG) for the opportunity to perform experiments at the Jungfraujoch. Additional thanks go to Oliver Appel (MPIC Mainz) for help with OPC error calculations, to Oliver Schlenczek (University Mainz) for cloud observations at the JFJ and to Udo Kästner (TROPOS) for his help during the measurements at the JFJ.

References

Abbatt, J. P., Benz, S., Cziczo, D. J., Kanji, Z., Lohmann, U., and Möhler, O.: Solid ammonium sulfate aerosols as ice nuclei: a pathway for cirrus cloud formation, Science, 313, 1770-1773, 2006.

Adler, G., Koop, T., Haspel, C., Taraniuk, I., Moise, T., Koren, I., Heiblum, R. H., and Rudich, Y.: Formation of highly porous aerosol particles by atmospheric freeze-drying in ice clouds, Proceedings of the National Academy of Sciences of the United States of America, 110, 20414-20419, 2013.

Atkinson, J. D., Murray, B. J., Woodhouse, M. T., Whale, T. F., Baustian, K. J., Carslaw, K. S., Dobbie, S., O'Sullivan, D., and Malkin, T. L.: The importance of feldspar for ice nucleation by mineral dust in mixed-phase clouds, Nature, 498, 355-358, 2013.

Bezdek, J. C., Ehrlich, R., and Full, W.: Fcm - the Fuzzy C-Means Clustering-Algorithm, Computers & Geosciences, 10, 191-203, 1984.

Brands, M., Kamphus, M., Böttger, T., Schneider, J., Drewnick, F., Roth, A., Curtius, J., Voigt, C., Borbon, A., Beekmann, M., Bourdon, A., Perrin, T., and Borrmann, S.: Characterization of a Newly Developed Aircraft-Based Laser Ablation Aerosol Mass Spectrometer (ALABAMA) and First Field Deployment in Urban Pollution Plumes over Paris During MEGAPOLI 2009, Aerosol Science and Technology, 45, 46-64, 2011.

Cantrell, W., and Heymsfield, A.: Production of Ice in Tropospheric Clouds: A Review, in: Bulletin of the American Meteorological Society, 6, 795-807, 2005.

Chen, Y., Kreidenweis, S. M., McInnes, L. M., Rogers, D. C., and DeMott, P. J.: Single particle analyses of ice nucleating aerosols in the upper troposphere and lower stratosphere, Geophysical Research Letters, 25, 1391-1394, 1998.

Chou, C., Stetzer, O., Weingartner, E., Jurányi, Z., Kanji, Z. A., and Lohmann, U.: Ice nuclei properties within a Saharan dust event at the Jungfraujoch in the Swiss Alps, Atmospheric Chemistry and Physics, 11, 4725-4738, 2011.

Corbin, J. C., Rehbein, P. J. G., Evans, G. J., and Abbatt, J. P. D.: Combustion particles as ice nuclei in an urban environment: Evidence from single-particle mass spectrometry, Atmospheric Environment, 51, 286-292, 2012.

Cozic, J., Mertes, S., Verheggen, B., Cziczo, D. J., Gallavardin, S. J., Walter, S., Baltensperger, U., and Weingartner, E.: Black carbon enrichment in atmospheric ice particle residuals observed in lower tropospheric mixed phase clouds, Journal of Geophysical Research-Atmospheres, 113, D15209, 2008a.

Cozic, J., Verheggen, B., Weingartner, E., Crosier, J., Bower, K. N., Flynn, M., Coe, H., Henning, S., Steinbacher, M., Henne, S., Collaud Coen, M., Petzold, A., and Baltensperger, U.: Chemical composition of free tropospheric aerosol for PM1 and coarse mode at high alpine site Jungfraujoch, Atmospheric Chemistry and Physics, 8, 407-423, 2008b.

Cziczo, D. J., DeMott, P. J., Brock, C., Hudson, P. K., Jesse, B., Kreidenweis, S. M., Prenni, A. J., Schreiner, J., Thomson, D. S., and Murphy, D. M.: A Method for Single Particle Mass Spectrometry of Ice Nuclei, Aerosol Science and Technology, 37, 460-470, 2003.

Cziczo, D. J., DeMott, P. J., Brooks, S. D., Prenni, A. J., Thomson, D. S., Baumgardner, D., Wilson, J. C., Kreidenweis, S. M., and Murphy, D. M.: Observations of organic species and atmospheric ice formation, Geophysical Research Letters, 31, L12116, 2004a.

Cziczo, D. J., Murphy, D. M., Hudson, P. K., and Thomson, D. S.: Single particle measurements of the chemical composition of cirrus ice residue during CRYSTAL-FACE, Journal of Geophysical Research-Atmospheres, 109, D04201, 2004b.

Cziczo, D. J., Stetzer, O., Worringen, A., Ebert, M., Weinbruch, S., Kamphus, M., Gallavardin, S. J., Curtius, J., Borrmann, S., Froyd, K. D., Mertes, S., Möhler, O., and Lohmann, U.: Inadvertent climate modification due to anthropogenic lead, Nature Geoscience, 2, 333-336, 2009.

Dall'Osto, M., Beddows, D. C. S., Kinnersley, R. P., and Harrison, R. M.: Characterization of individual airborne particles by using aerosol time-of-flight mass spectrometry at Mace Head, Ireland, Journal of Geophysical Research, 109, D21302, 2004.

Dall'Osto, M., and Harrison, R. M.: Chemical characterisation of single airborne particles in Athens (Greece) by ATOFMS, Atmospheric Environment, 40, 7614-7631, 2006.

Dall’Osto, M., Harrison, R. M., Highwood, E. J., O’Dowd, C., Ceburnis, D., Querol, X., and Achterberg, E. P.: Variation of the mixing state of Saharan dust particles with atmospheric transport, Atmospheric Environment, 44, 3135-3146, 2010.

de Foy, B., Smyth, A. M., Thompson, S. L., Gross, D. S., Olson, M. R., Sager, N., and Schauer, J. J.: Sources of nickel, vanadium and black carbon in aerosols in Milwaukee, Atmospheric Environment, 59, 294-301, 2012.

DeCarlo, P. F., Slowik, J. G., Worsnop, D. R., Davidovits, P., and Jimenez, J. L.: Particle Morphology and Density Characterization by Combined Mobility and Aerodynamic Diameter Measurements. Part 1: Theory, Aerosol Science and Technology, 38, 1185-1205, 2004.

DeMott, P. J., Rogers, D. C., Kreidenweis, S. M., Chen, Y., Twohy, C. H., Baumgardner, D., Heymsfield, A. J., and Chan, K. R.: The role of heterogeneous freezing nucleation in upper tropospheric clouds: Inferences from SUCCESS, Geophysical Research Letters, 25, 1387-1390, 1998.

DeMott, P. J., Chen, Y., Kreidenweis, S. M., Rogers, D. C., and Sherman, D. E.: Ice formation by black carbon particles, Geophysical Research Letters, 26, 2429-2432, 1999.

DeMott, P. J., Cziczo, D. J., Prenni, A. J., Murphy, D. M., Kreidenweis, S. M., Thomson, D. S., Borys, R., and Rogers, D. C.: Measurements of the concentration and composition of nuclei for cirrus formation, Proceedings of the National Academy of Sciences of the United States of America, 100, 14655-14660, 2003a.

DeMott, P. J., Sassen, K., Poellot, M. R., Baumgardner, D., Rogers, D. C., Brooks, S. D., Prenni, A. J., and Kreidenweis, S. M.: African dust aerosols as atmospheric ice nuclei, Geophysical Research Letters, 30, 10.1029/2003gl017410, 2003b.

DeMott, P. J., Prenni, A. J., Liu, X., Kreidenweis, S. M., Petters, M. D., Twohy, C. H., Richardson, M. S., Eidhammer, T., and Rogers, D. C.: Predicting global atmospheric nuclei distributions and their impacts on climate, Proceedings of the National Academy of Sciences of the United States of America, 107, 11217-11222, 2010.

Diehl, K., Quick, C., Matthias-Maser, S., Mitra, S. K., and Jaenicke, R.: The ice nucleating ability of pollen - Part I: Laboratory studies in deposition and condensation freezing mode, Atmospheric Research, 58, 75-87, 2001.

Diehl, K., and Wurzler, S.: Air parcel model simulations of a convective cloud: Bacteria acting as immersion ice nuclei, Atmospheric Environment, 44, 4622-4628, 2010.

Diehl, K., Debertshäuser, M., Eppers, O., Schmithüsen, H., Mitra, S. K., and Borrmann, S.: Particle surface area dependence of mineral dust in immersion freezing mode: investigations with freely suspended drops in an acoustic levitator and a vertical wind tunnel, Atmospheric Chemistry and Physics 14, 12343-12355, 2014.

Draxler, R. R., and Rolph, G. D.: HYSPLIT (HYbrid Single-Particle Lagrangian Integrated Trajectory) Model access via NOAA ARL READY Website (http://ready.arl.noaa.gov/HYSPLIT.php), NOAA Air Resources Laboratory, Silver Spring, MD, 2012.

Dymarska, M., Murray, B. J., Sun, L., Eastwood, M. L., Knopf, D. A., and Bertram, A. K.: Deposition ice nucleation on soot at temperatures relevant for the lower troposphere, Journal of Geophysical Research-Atmospheres, 111, D04204, 2006.

Ebert, M., Worringen, A., Benker, N., Mertes, S., Weingartner, E., and Weinbruch, S.: Chemical composition and mixing-state of ice residuals sampled within mixed phase clouds, Atmospheric Chemistry and Physics, 11, 2805-2816, 2011.

Fergenson, D. P., Pitesky, M. E., Tobias, H. J., Steele, P. T., Czerwieniec, G. A., Russell, S. C., Lebrilla, C. B., Horn, J. M., Coffee, K. R., Srivastava, A., Pillai, S. P., Shih, M.-T. P., Hall, H. L., Ramponi, A. J., Chang, J. T., Langlois, R. G., Estacio, P. L., Hadley, R. T., Frank, M., and Gard, E. E.: Reagentless Detection and Classification of Individual Bioaerosol Particles in Seconds, Analytic Chemistry, 76, 373-378, 2004.

Frank, M., Gard, E. E., Tobias, H. J., Adams, K. L., Bogan, M. J., Coffee, K. R., Farquar, G. R., Fergenson, D. P., Martin, S. I., Pitesky, M., Riot, V. J., Srivastava, A., Steele, P. T., and Williams, A. M.: Single-Particle Aerosol Mass Spectrometry (SPAMS) for High-Throughput and Rapid Analysis of Biological Aerosols and Single Cells, in: Rapid Characterization of Microorganisms by Mass Spectrometry, American Chemical Society, Washington, DC, 161-196, 2011.

Froyd, K. D., Murphy, D. M., Lawson, P., Baumgardner, D., and Herman, R. L.: Aerosols that form subvisible cirrus at the tropical tropopause, Atmospheric Chemistry and Physics, 10, 209-218, 2010.

Fukuta, N., and Takahashi, T.: The Growth of Atmospheric Ice Crystals: A Summary of Findings in Vertical Supercooled Cloud Tunnel Studies, Journal of the Atmospheric Sciences, 56, 1963-1979, 1999.

Gerber, H.: Microphysics of Marine Stratocumulus Clouds with Two Drizzle Modes, Journal of the Atmospheric Sciences, 53, 1649-1662, 1996.

Hartmann, S., Niedermeier, D., Voigtländer, J., Clauss, T., Shaw, R. A., Wex, H., Kiselev, A., and Stratmann, F.: Homogeneous and heterogeneous ice nucleation at LACIS: operating principle and theoretical studies, Atmospheric Chemistry and Physics, 11, 1753-1767, 2011.

Heim, M., Mullins, B. J., Umhauer, H., and Kasper, G.: Performance evaluation of three optical 30 particle counters with an efficient "multimodal" calibration method, Journal of Aerosol Science, 39, 1019-1031, 2008.

Hinz, K.-P., Greweling, M., Drews, F., and Spengler, B.: Data Processing in On-line Laser Mass Spectrometry of Inorganic, Organic, or Biological Airborne Particles, American Society for Mass Spectrometry, 10, 648-660, 1999.

Hoose, C., Kristjánsson, J. E., and Burrows, S. M.: How important is biological ice nucleation in clouds on a global scale?, Environmental Research Letters, 5, 024009, 10.1088/1748-9326/5/2/024009, 2010.

Hoose, C., and Möhler, O.: Heterogeneous ice nucleation on atmospheric aerosols: a review of results from laboratory experiments, Atmospheric Chemistry and Physics, 12, 9817-9854, 2012.

Huang, M., Xia, Z., Wang, H., Zeng, Q., and Wang, Q.: The range of the value for the fuzzifier of the fuzzy c-means algorithm, Pattern Recognition Letters, 33, 2280-2284, 2012.

Huang, M., Hao, L., Guo, X., Hu, C., Gu, X., Zhao, W., Wang, Z., Fang, L., and Zhang, W.: Characterization of secondary organic aerosol particles using aerosol laser time-of-flight mass spectrometer coupled with FCM clustering algorithm, Atmospheric Environment, 64, 85-94, 2013.

Kamphus, M., Ettner-Mahl, M., Brands, M., Curtius, J., Drewnick, F., and Borrmann, S.: Comparison of Two Aerodynamic Lenses as an Inlet for a Single Particle Laser Ablation Mass Spectrometer, Aerosol Science and Technology, 42, 970-980, 2008.

Kamphus, M., Ettner-Mahl, M., Klimach, T., Drewnick, F., Keller, L., Cziczo, D. J., Mertes, S., Borrmann, S., and Curtius, J.: Chemical composition of ambient aerosol, ice residues and cloud droplet residues in mixed-phase clouds: single particle analysis during the Cloud and Aerosol Characterization Experiment (CLACE 6), Atmospheric Chemistry and Physics, 10, 8077-8095, 2010.

Kandler, K., Lieke, K., Benker, N., Emmel, C., Küpper, M., Müller-Ebert, D., Ebert, M., Scheuvens, D., Schladitz, A., Schütz, L., and Weinbruch, S.: Electron microscopy of particles collected at Praia, Cape Verde, during the Saharan Mineral Dust Experiment: particle chemistry, shape, mixing state and complex refractive index, Tellus Series B - Chemical and Physical Meteorology, 63, 475-496, 2011.

Kaye, P. H., Hirst, E., Greenaway, R. S., Ulanowski, Z., Hesse, E., DeMott, P. J., Saunders, C., and Connolly, P.: Classifying atmospheric ice crystals by spatial light scattering, Optics Letters, 33, 1545-1547, 2008.

Klimach, T.: Chemische Zusammensetzung der Aerosole - Design und Datenauswertung eines Einzelpartikel-Laserablationsmassenspektrometers, PhD thesis, University of Mainz, Germany, 2012.

Koop, T., Luo, B. P., Tsias, A., and Peter, T.: Water activity as the determinant for homogeneous ice nucleation in aqueous solutions, Nature, 406, 611-614, 2000.

Kupiszewski, P., Weingartner, E., Vochezer, P., Bigi, A., Rosati, B., Gysel, M., Schnaiter, M., and Baltensperger, U.: The Ice Selective Inlet: a novel technique for exclusive extraction of pristine ice crystals in mixed-phase clouds, Atmospheric Measurement Techniques Discussions, 7, 12481-12515, 2014.

Lance, S., Brock, C. A., Rogers, D., and Gordon, J. A.: Water droplet calibration of the Cloud Droplet Probe (CDP) and in-flight performance in liqiud, ice and mixed-phase clouds during ARCPAC, Atmospheric Measurement Techniques, 3, 1683-1706, 2010.

Liu, P., Ziemann, P. J., Kittelson, D. B., and McMurry, P. H.: Generating Particle Beams of Controlled Dimensions and Divergence: II. Experimental Evaluation of Particle Motion in Aerodynamic Lenses and Nozzle Expansions, Aerosol Science and Technology, 22, 314-324, 1995a.

Liu, P., Ziemann, P. J., Kittelson, D. B., and McMurry, P. H.: Generating Particle Beams of Controlled Dimensions and Divergence: I. Theory of Particle Motion in Aerodynamic Lenses and Nozzle Expansions, Aerosol Science and Technology, 22, 293-313, 1995b.

Liu, P. S. K., Deng, R., Smith, K. A., Williams, L. R., Jayne, J. T., Canagaratna, M. R., Moore, K., Onasch, T. B., Worsnop, D. R., and Deshler, T.: Transmission Efficiency of an Aerodynamic Focusing Lens System: Comparison of Model Calculations and Laboratory Measurements for the Aerodyne Aerosol Mass Spectrometer, Aerosol Science and Technology, 41, 721-733, 2007.

Lohmann, U., and Feichter, J.: Global indirect aerosol effects: a review, Atmospheric Chemistry and Physics, 5, 715-737, 2005.

Mertes, S., Lehmann, K., Nowak, A., Massling, A., and Wiedensohler, A.: Link between aerosol hygroscopic growth and droplet activation observed for hill-capped clouds at connected flow conditions during FEBUKO, Atmospheric Environment, 39, 4247-4256, 2005.

Mertes, S., Verheggen, B., Walter, S., Connolly, P., Ebert, M., Schneider, J., Bower, K. N., Cozic, J., Weinbruch, S., Baltensperger, U., and Weingartner, E.: Counterflow Virtual Impactor Based Collection of Small Ice Particles in Mixed-Phase Clouds for the Physico-Chemical Characterization of Tropospheric Ice Nuclei: Sampler Description and First Case Study, Aerosol Science and Technology, 41, 848-864, 2007.

Möhler, O., DeMott, P. J., Vali, G., and Levin, Z.: Microbiology and atmospheric processes: the role of biological particles in cloud physics, Biogeoscience, 4, 1059-1071, 2007.

Möhler, O., Georgakopoulos, D. G., Morris, C. E., Benz, S., Ebert, V., Hunsmann, S., Saathoff, H., Schnaiter, M., and Wagner, R.: Heterogeneous ice nucleation activity of bacteria: new laboratory experiments at simulated cloud conditions, Biogeosciences 5, 1425-1435, 2008.

Murphy, D. M., Cziczo, D. J., Hudson, P. K., Thomson, D. S., Wilson, J. C., Kojima, T., and Buseck, P. R.: Particle Generation and Resuspension in Aircraft Inlets when Flying in Clouds, Aerosol Science and Technology, 38, 401-409, 2004.

Murphy, D. M., Hudson, P. K., Cziczo, D. J., Gallavardin, S., Froyd, K. D., Johnston, M. V., Middlebrook, A. M., Reinard, M. S., Thomson, D. S., Thornberry, T., and Wexler, A. S.: Distribution of lead in single atmospheric particles, Atmospheric Chemistry and Physics, 7, 3195-3210, 2007.

Murray, B. J., Wilson, T. W., Dobbie, S., Cui, Z., Al-Jumur, S. M. R. K., Möhler, O., Schnaiter, M., Wagner, R., Benz, S., Niemand, M., Saathoff, H., Ebert, V., Wagner, S., and Kärcher, B.: Heterogeneous nucleation of ice particles on glassy aerosols under cirrus conditions, Nature Geoscience, 3, 233-237, 2010.

Murray, B. J., Broadley, S. L., Wilson, T. W., Atkinson, J. D., and Wills, R. H.: Heterogeneous freezing of water droplets containing kaolinite particles, Atmospheric Chemistry and Physics, 11, 4191-4207, 2011.

Murray, B. J., O'Sullivan, D., Atkinson, J. D., and Webb, M. E.: Ice nucleation by particles immersed in supercooled cloud droplets, Chemical Society reviews, 41, 6519-6554, 2012.

Pratt, K. A., DeMott, P. J., French, J. R., Wang, Z., Westphal, D. L., Heymsfield, A. J., Twohy, C. H., Prenni, A. J., and Prather, K. A.: In situ detection of biological particles in cloud ice-crystals, Nature Geoscience, 2, 398-401, 2009.

Pratt, K. A., Heymsfield, A. J., Twohy, C. H., Murphy, S. M., DeMott, P. J., Hudson, J. G., Subramanian, R., Wang, Z., Seinfeld, J. H., and Prather, K. A.: In Situ Chemical Characterization of Aged Biomass-Burning Aerosols Impacting Cold Wave Clouds, Journal of the Atmospheric Sciences, 67, 2451-2468, 2010.

Pratt, K. A., and Prather, K. A.: Aircraft measurements of vertical profiles of aerosol mixing states, Journal of Geophysical Research-Atmospheres, 115, D11305, 2010.

Prenni, A. J., Petters, M. D., Kreidenweis, S. M., Heald, C. L., Martin, S. T., Artaxo, P., Garland, R. M., Wollny, A. G., and Pöschl, U.: Relative roles of biogenic emissions and Saharan dust as ice nuclei in the Amazon basin, Nature Geoscience, 2, 402-405, 2009.

Pruppacher, H. R., and Klett, J. D.: Microphysics of Clouds and Precipitation, Kluwer Acedemic Publishers, Dodrecht, 2010.

Rogers, D. C., DeMott, P. J., Kreidenweis, S. M., and Chen, Y. L.: Measurements of ice nucleating aerosols during SUCCESS, Geophysical Research Letters, 25, 1383-1386, 1998.

Rolph, G. D.: Real-time Environmental Applications and Display sYstems (READY) Website (http://ready.arl.noaa.gov), NOAA Air Resources Laboratory, Silver Spring, MD, 2014.

Rosati, B., Wehrle, G., Gysel, M., Zieger, P., Baltensperger, U., and Weingartner, E.: The white-light humidified optical particle spectrometer (WHOPS) - a novel airborne system to characterize aerosol hygroscopicity, Atmospheric Measurement Techniques, 8, 2015.

Roth, A.: Untersuchungen von Aerosolpartikeln und Wolkenresidualpartikeln mittels Einzelpartikel-Massenspektrometrie und optischen Methoden, PhD thesis, University of Mainz, Germany, 2014.

Schneider, J., Weimer, S., Drewnick, F., Borrmann, S., Helas, G., Gwaze, P., Schmid, O., Andreae, M. O., and Kirchner, U.: Mass spectrometric analysis and aerodynamic properties of various types of combustion-related aerosol particles, International Journal of Mass Spectrometry, 258, 37-49, 2006.

Seinfeld, J. H., and Pandis, S. N.: Atmospheric Chemistry and Physics: From Air Pollution to Climate Change, John Wiley & Sons, Inc., New Jersey, 2006.

Slowik, J. G., Stainken, K., Davidovits, P., Williams, L. R., Jayne, J. T., Kolb, C. E., Worsnop, D. R., Rudich, Y., DeCarlo, P. F., and Jimenez, J. L.: Particle Morphology and Density Characterization by Combined Mobility and Aerodynamic Diameter Measurements. Part 2: Application to Combustion-Generated Soot Aerosols as a Function of Fuel Equivalence Ratio, Aerosol Science and Technology, 38, 1206-1222, 2004.

Steinke, I., Hoose, C., Möhler, O., Connolly, P., and Leisner, T.: A new temperature- and humidity-dependent surface site density approach for deposition ice nucleation, Atmospheric Chemistry and Physics 15, 3703-3717, 2015.

Tenberken-Pötzsch, B., Schwikowski, M., and Gäggeler, H. W.: A method to sample and separate ice crystals and supercooled cloud droplets in mixed phased clouds for subsequent chemical analysis, Atmospheric Environment, 34, 3629-3633, 2000.

Tobo, Y., DeMott, P. J., Hill, T. C. J., Prenni, A. J., Swoboda-Colberg, N. G., Franc, G. D., and Kreidenweis, S. M.: Organic matter matters for ice nuclei of agricultural soil origin, Atmospheric Chemistry and Physics, 14, 8521-8531, 2014.

Trimborn, A.: Online analysis of atmospheric particles with a transportable laser mass spectrometer during LACE 98, Journal of Geophysical Research, 107, 8132, 2002.

Trimborn, A., Hinz, K.-P., and Spengler, B.: Online analysis of atmospheric particles with a transportable laser mass spectrometer during LACE 98, Journal of Geophysical Research, 107, 8132, 2002.

Twohy, C. H., DeMott, P. J., Pratt, K. A., Subramanian, R., Kok, G. L., Murphy, S. M., Lersch, T., Heymsfield, A. J., Wang, Z., Prather, K. A., and Seinfeld, J. H.: Relationships of

Biomass-Burning Aerosols to Ice in Orographic Wave Clouds, Journal of the Atmospheric Sciences, 67, 2437-2450, 2010.

Vali, G., DeMott, P. J., Möhler, O., and Whale, T. F.: Ice nucleation terminology, Atmospheric Chemistry and Physics Discussion, 14, 22155-22162, 2014.

Vochezer, P., Järvinen, E., Wagner, R., Kupiszewski, P., Leisner, T., and Schnaiter, M.: In situ characterization of mixed phase clouds using the Small Ice Detector and Particle Phase Discriminator, submitted to Atmospheric Measurement Techniques 2015.

von Blohn, N., Mitra, S. K., Diehl, K., and Borrmann, S.: The ice nucleating ability of pollen: Part III: New laboratory studies in immersion and contact freezing modes including more pollen types, Atmospheric Research, 78, 182-189, 2005.

von der Weiden, S.-L., Drewnick, F., and Borrmann, S.: Particle Loss Calculator - a new software tool for the assessment of the performance of aerosol inlet systems, Atmospheric Measurement Techniques, 2, 479-494, 2009.

Weinbruch, S., Worringen, A., Ebert, M., Scheuvens, D., Kandler, K., Pfeffer, U., and Bruckmann, P.: A quantitative estimation of the exhaust, abrasion and resuspension components of particulate traffic emissions using electron microscopy, Atmospheric Environment, 99, 175-182, 2014.

Weingartner, E., Nyeki, S., and Baltensperger, U.: Seasonal and diurnal variation of aerosol size distributions (10<D<750 nm) at a high-alpine site (Jungfraujoch 3580 m asl), Journal of Geophysical Research-Atmospheres, 104, 26809-26820, 1999.

Wendisch, M.: A Quantitative Comparison of Ground-Based FSSP and PVM Measurements, Journal of Atmospheric and Oceanic Technology, 15, 887-900, 1998.

Wise, M. E., Baustian, K. J., Koop, T., Freedman, M. A., Jensen, E. J., and Tolbert, M. A.: Depositional ice nucleation onto crystalline hydrated NaCl particles: a new mechanism for ice formation in the troposphere, Atmospheric Chemistry and Physics, 12, 1121-1134, 2012.

Worringen, A., Kandler, K., Benker, N., Dirsch, T., Mertes, S., Schenk, L., Kästner, U., Frank, F., Nillius, B., Bundke, U., Rose, D., Curtius, J., Kupiszewski, P., Weingartner, E., Vochezer, P., Schneider, J., Schmidt, S., Weinbruch, S., and Ebert, M.: Single-particle characterization of ice-nucleating particles and ice particle residuals sampled by three different techniques, Atmospheric Chemistry and Physics, 15, 4161-4178, 2015.

Zelenyuk, A., Cai, Y., and Imre, D.: From Agglomerates of Spheres to Irregularly Shaped Particles: Determination of Dynamic Shape Factors from Measurements of Mobility and Vacuum Aerodynamic Diameters, Aerosol Science and Technology, 40, 197-217, 2006.

Table 1: Cloud events during which measurements were taken behind Ice-CVI or ISI, along with the ALABAMA sampling time, the number of the measured spectra, the evaluation of the Ice-CVI-sampling-periods and the weather conditions and cloud formation during these events. The times of each cloud event based $^{a)}$ on the particle counter operated behind the Ice-CVI or $^{b)}$ on the liquid water content measured by two PVM instruments and a CDP outside the laboratory.

Event	**Sampling time (local time)**	**Inlet**	**Number of spectra**	**Classification of the Ice CVI-sampling-periods**	**Weather conditions & clouds**
1	$^{a)}$22.01.2013 01:48 – 12:02	CVI	174	++	Warm front occlusive low pressure system; $\overline{T}$ = -19.2 °C; wind direction wd = 325°; wind speed $\bar{v}$ = 8.1 ms^{-1}
2	$^{a)}$27.01.2013 16:27 – 28.01.2013 09:44	CVI	78	++	Occlusive frontal system, Ns; $\overline{T}$ = -12.7 °C; wd = 318°;$\bar{v}$ = 8.4 ms^{-1}
3	$^{a)}$1. 29.01.2013 04:30 – 13:57 2. 29.01.2013 19:27 – 19:52	CVI	20 3	++ ++	Unstable warm front; first Ns than Cb; $\overline{T}$ = -7.8 °C; wd = 320°; $\bar{v}$ = 12,6 ms^{-1}
4	$^{a)}$30.01.2013 16:14 – 31.01.2013 01:03	CVI	39	++	Squall line at cold front; Cb; $\overline{T}$ = -8.6 °C; wd = 323°; $\bar{v}$ = 16.9 ms^{-1}
5	$^{a)}$1. 01.02.2013 17:22 – 02.02.2013 01:30 2. 02.02.2013 01:30 – 13:07 3. 02.02.2013 17:58 – 03.02.2013 01:00 4. 03.02.2013 01:00 – 10:45	CVI	134 701 209 73	++ +- +- ++	31.01.: cellular convection; Cu; $\overline{T}$ = -12,5°C; wd = 324°; $\bar{v}$ = 17.7 ms^{-1} 01.02. – 02.02.: frontal wave; Ns and Cb; $\overline{T}$ = -13.7°C; wd = 319°; $\bar{v}$ = 13.4 ms^{-1} Until 03.02. cellular convection; Cb; $\overline{T}$ = -23.1°C; wd = 308°; $\bar{v}$ = 9.7 ms^{-1}

	b)1. 31.01.2013 18:55 – 21:42	ISI	9		
	2. 01.02.2013 01:53 – 11:05		18		
6	a)1. 05.02.2013 19:06 – 23:00	CVI	24	++	Squall line at postfrontal convergence line; Cb; $\overline{T}$ = -19.8°C; wd = 331°; $\overline{v}$ = 10.5 ms^{-1}
	2. 05.02.2013 23:00 – 06.02.2013 04:20		42	+-	
	3. 06.02.2013 04:20 – 05:00		3	++	
7	a)1. 06.02.2013 08:33 – 11:00	CVI	26	+-	06.02: Convective dominating low-pressure vortex; Cb; $\overline{T}$ = -24.3°C; wd = 310°; $\overline{v}$ = 8.0 ms^{-1} From 07.02. on: cellular convection; Cu; $\overline{T}$ = -20.8°C; wd = 324°; $\overline{v}$ = 7.6 ms^{-1}
	2. 06.02.2013 11:00 – 12:30		4	++	
	3. 06.02.2013 12:30 – 14:56		15	+-	
	4. 06.02.2013 15:44 – 15:53		3	+-	
	5. 06.02.2013 23:32 – 07.02.2013 04:30		8	++	
	6. 07.02.2013 04:30 – 08:45		6	+-	
	7. 07.02.2013 08:45 – 09:49		2	++	
	8. 07.02.2013 20:29 – 08.02.2013 05:50		31	+-	
	9. 08.02.2013 05:50 – 09:20		2	++	
8	a)1. 09.02.2013 01:09 – 02:30	CVI	4	++	Diamond dust and cellular convection at convergence line; Ci, Cu (Cb); $\overline{T}$ = -26.7 °C; wd = 316°; $\overline{v}$ = 7.2 ms^{-1}
	2. 09.02.2013 02:30 – 09:00		32	+-	
	3. 09.02.2013 09:00 – 09:41		3	++	
9	a)10.02.2013 18:10 – 18:24	CVI	2	++	Approaching warm front; Ci, Cs, As; $\overline{T}$ = -15.7°C; wd = 324°; $\overline{v}$ = 9.5 ms^{-1}
10	a)1. 11.02.2013 08:03 – 10:31	CVI	1	++	Warm front; Ns; $\overline{T}$ = -18.7°C; wd = 227°; $\overline{v}$ = 6.6 ms^{-1}
	2. 11.02.2013 15:08 – 12.02.2013 06:11		11	++	

11	[a]12.02.2013 16:07 – 13.02.2013 01:33	CVI	8	++	Back of a low with northeast stream; Ns, Ac, As; $\overline{T}$ = -20.1°C; wd = 319°; $\bar{v}$ = 7.9 ms^{-1}
12	[b]15.02.2013 01:17 – 09:10	ISI	114		Low pressure system; As, Cu, Cb, Ac; $\overline{T}$ = -16.9 °C; wd = 322°; $\bar{v}$ = 7.7 ms^{-1}
13	[a]19.02.2013 16:46 – 20.02.2013 16:47	CVI	1	++	Cold front from North; Ac, Ns, Sc, Cu; $\overline{T}$ = -14.3 °C; wd = 321°; $\bar{v}$ = 8.2 ms^{-1}
14	[b]24.02.2013 06:57 – 24.02.2013 09:31	ISI	3		Approaching warm front with precipitation; Cs, As, Ns; $\overline{T}$ = -20.4 °C, wd = 150°; $\bar{v}$ = 8.5 ms^{-1}

Ac: altocumulus
As: altostratus
Cb: cumulonimbus
Ci: cirrus
Cs: cirrostratus
Cu: cumulus
Ns: nimbostratus
Sc: stratocumulus

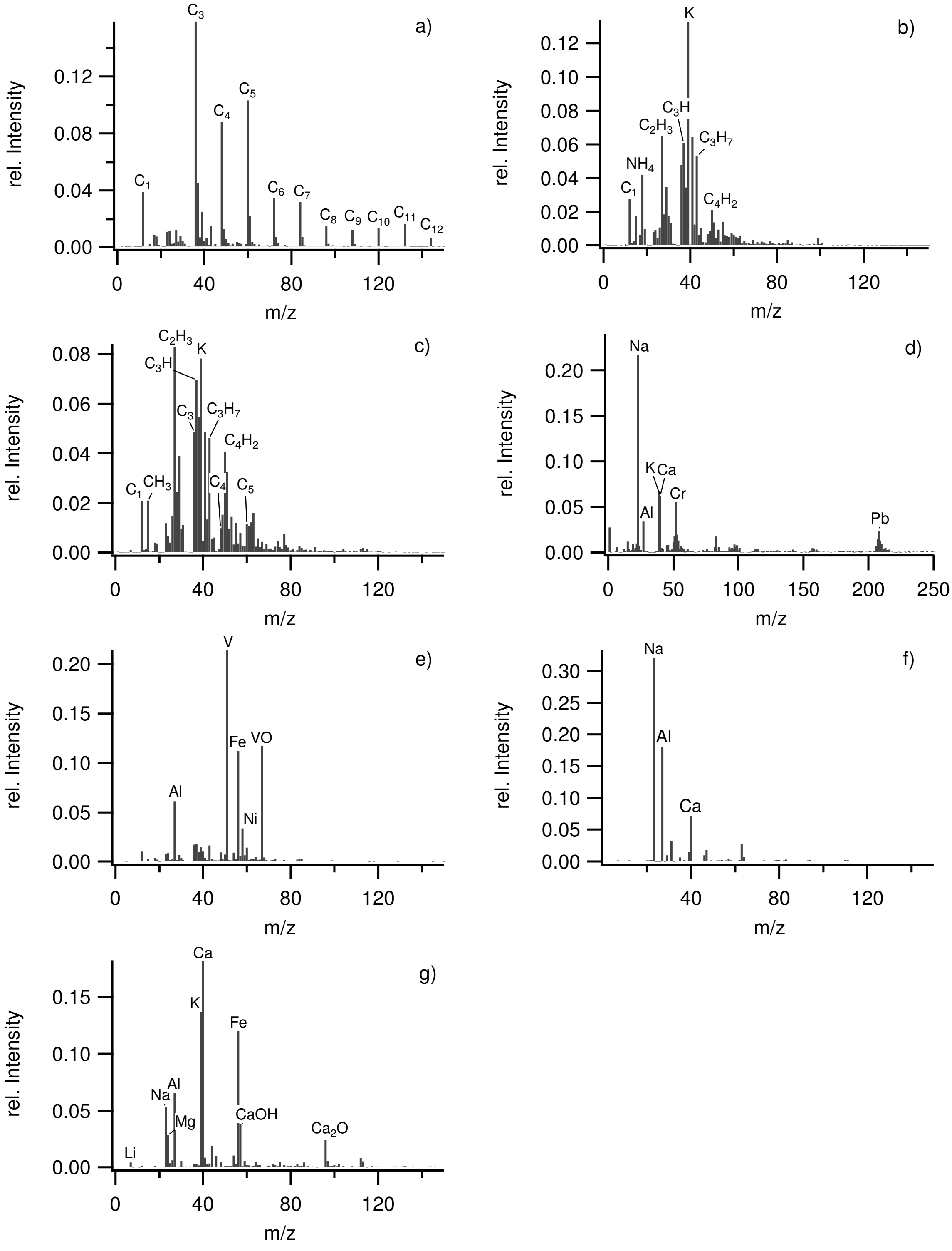

Figure 1: Average mass spectra of each particle type. a) black carbon; b) organic carbon; c) black carbon internally mixed with organic carbon; d) lead containing particles; e) industrial metals; f) Bio/Min/Sal; g) minerals

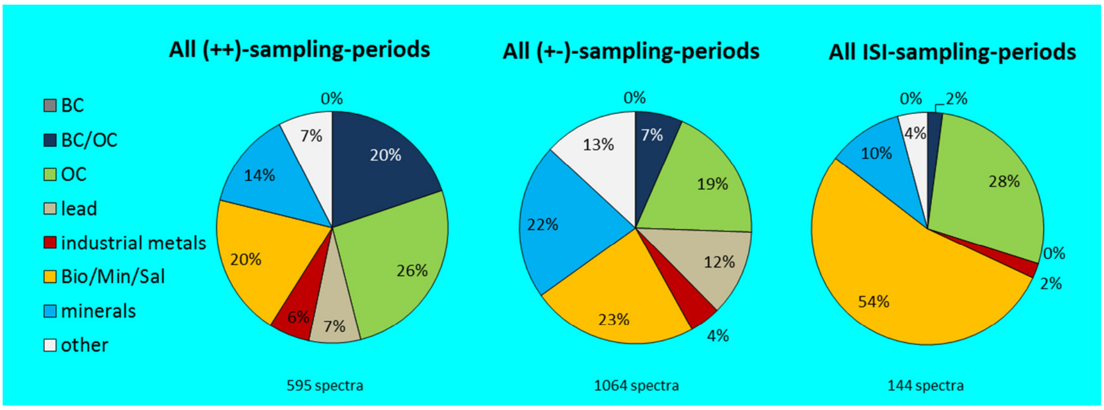

Figure 2: Results of the IPR composition analysis. Left and middle: measurements behind the Ice-CVI (left: all (++)-sampling-periods; middle: all (+-)-sampling-periods). Right: IPR composition measured behind the ISI.

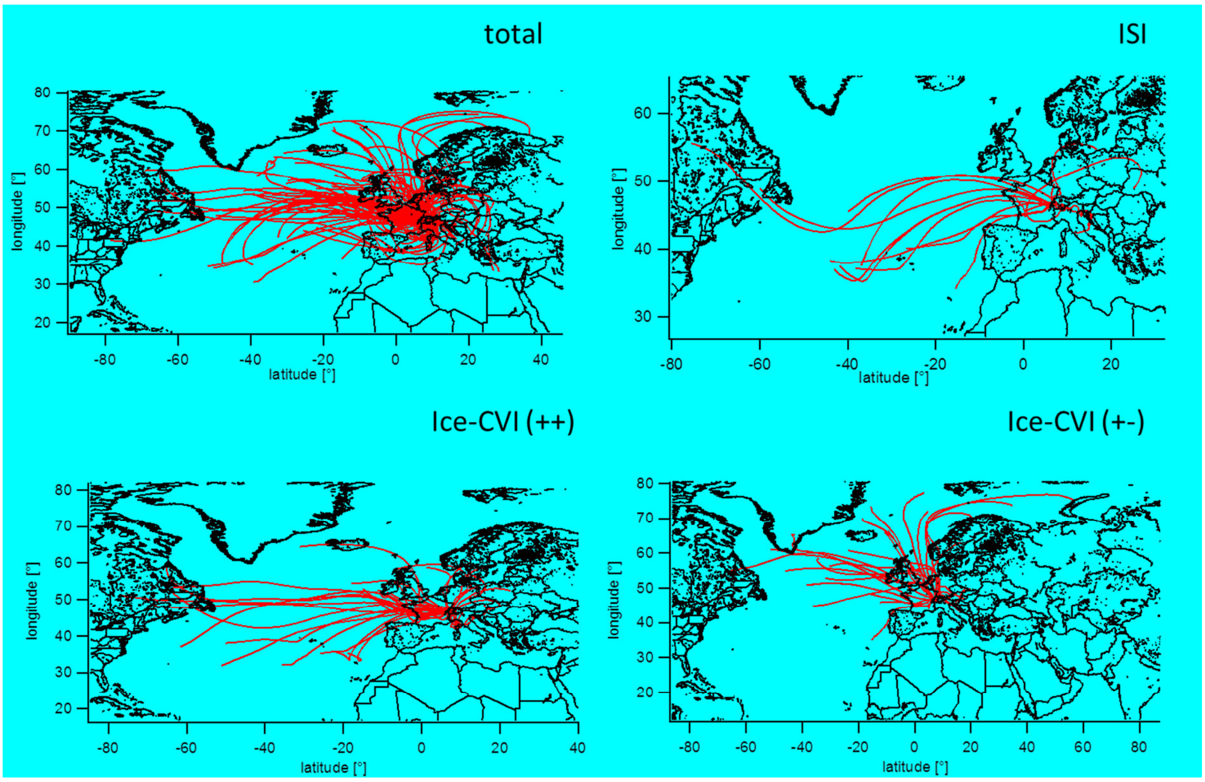

Figure 3: 72 h backward trajectories calculated with CRISP/HYSPLIT (one trajectory every 6 h)

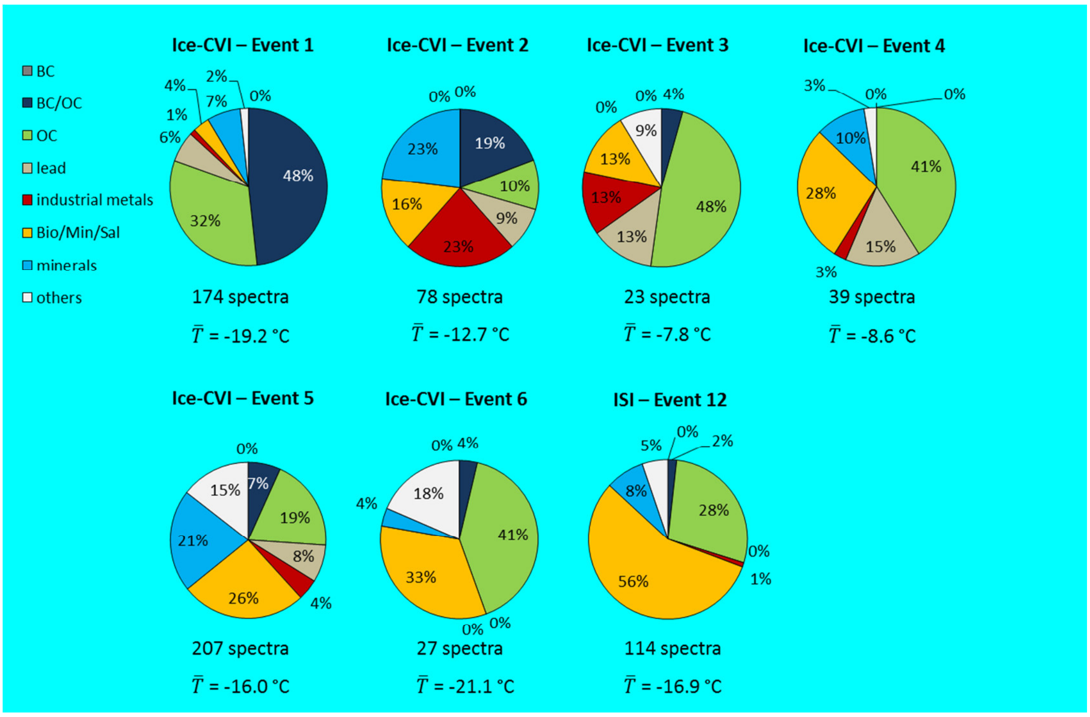

Figure 4: Comparison of the composition analysis of seven events measuring behind the Ice-CVI (all (++)-sampling-periods, Event 1: 22.01.2013 01:48 – 12:02; Event 2: 27.01.2013 16:27 – 28.01.2013 09:44; Event 3: 3.1 29.01.2013 04:30 – 13:57; 3.2 29.01.2013 19:27 – 19:52; Event 4: 30.01.2013 16:14 – 31.01.2013 01:03; Event 5: 5.1 01.02.2013 17:22 – 02.02.2013 01:30; 5.4 03.02.2013 01:00 – 10:45 and Event 6: 6.1 05.02.2013 19:06 – 23:00; 6.3 06.02.2013 04:20 – 05:00) and the ISI (Event 12: 15.02.2013 01:17 – 09:10) together with the corresponding average temperature during each event.

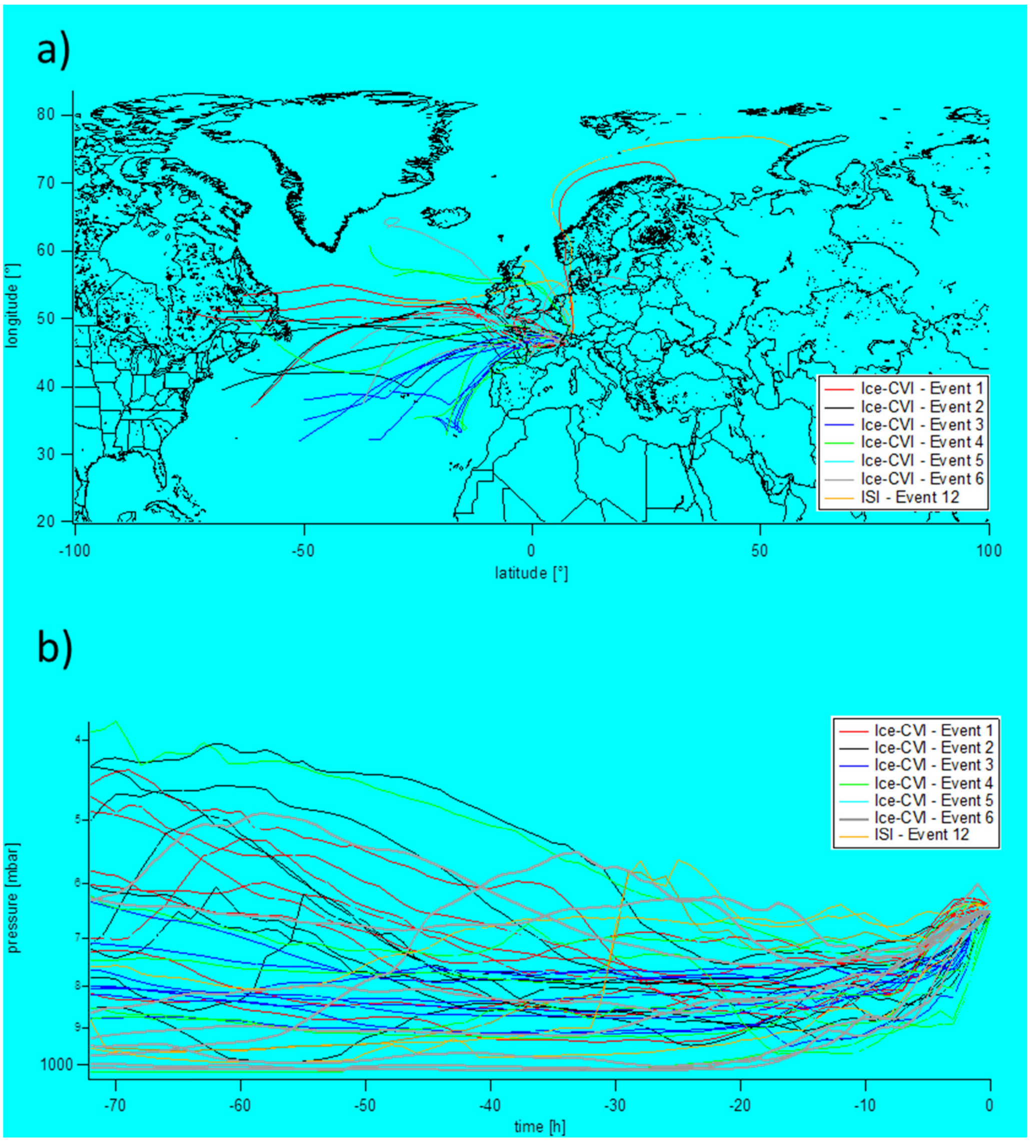

Figure 5: a) 72 h backward trajectories (one trajectory every three hours) calculated with CRISP for each event. b) The altitudes of air masses reaching the Jungfraujoch as a function of time, converted to pressure units.

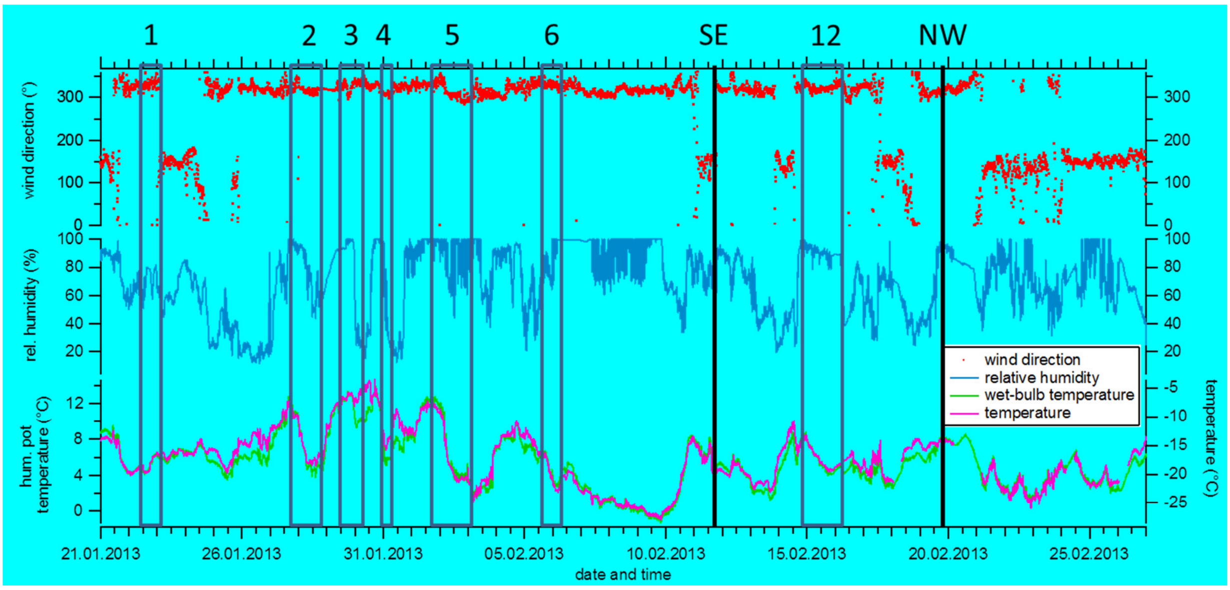

Figure 6: Wind direction, relative humidity, potential wet-bulb temperature and temperature over the whole measurement period (data from MeteoSwiss at the JFJ station). Black lines denote the events with different air mass origin (discussed in section 3.4). Events highlighted with blue bars denote the 7 different events from Section 2.1.1.

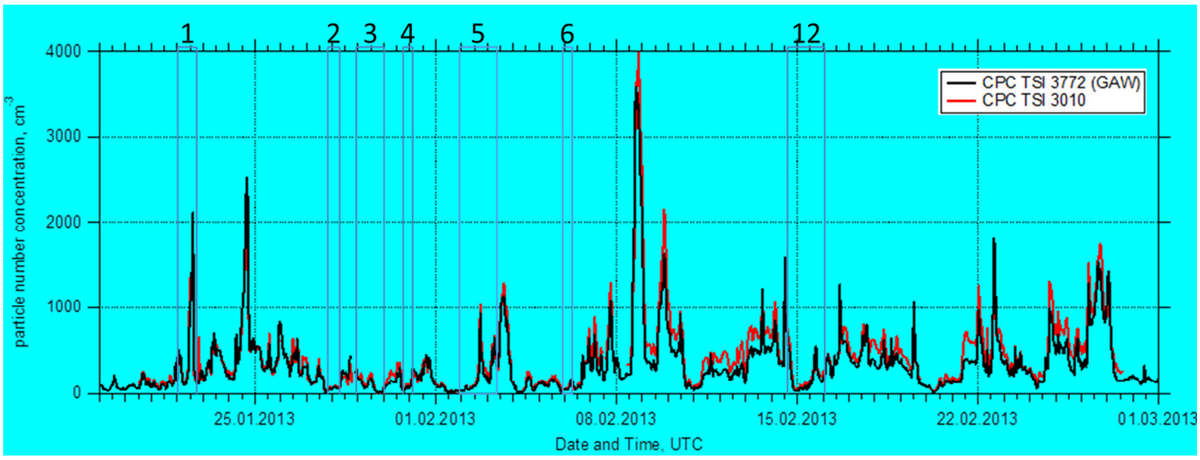

Figure 7: Particle number concentrations measured during the INUIT-JFJ/CLACE 2013 campaign by two different condensation particle counters (CPC): The GAW-CPC which is located directly behind the total inlet, and a TSI 3010 that was operated with a much longer sampling line (approx. 7 m) next to one of the aerosol mass spectrometers. Short elevated concentrations indicate local emissions. Events highlighted with blue bars denote the 7 different events from Section 2.1.1

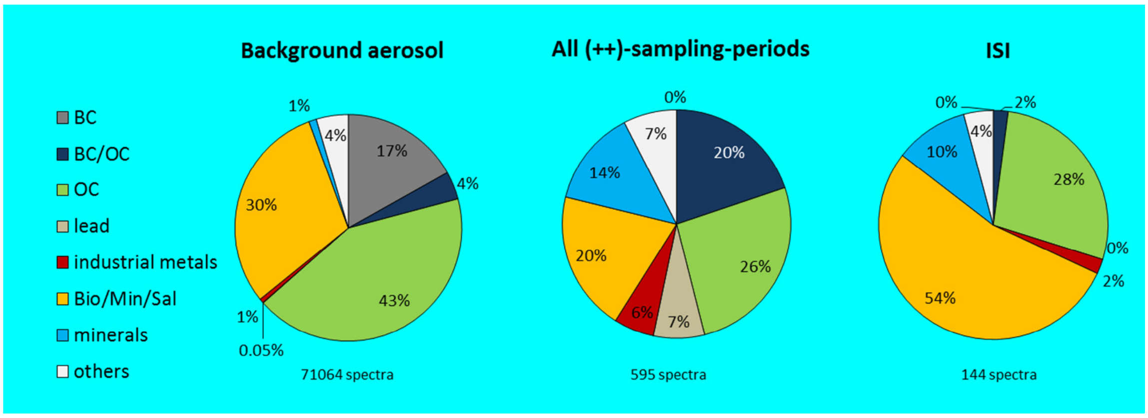

Figure 8: Comparison between the chemical composition of background aerosol particles (left) and IPR measured behind Ice-CVI (middle) and ISI (right).

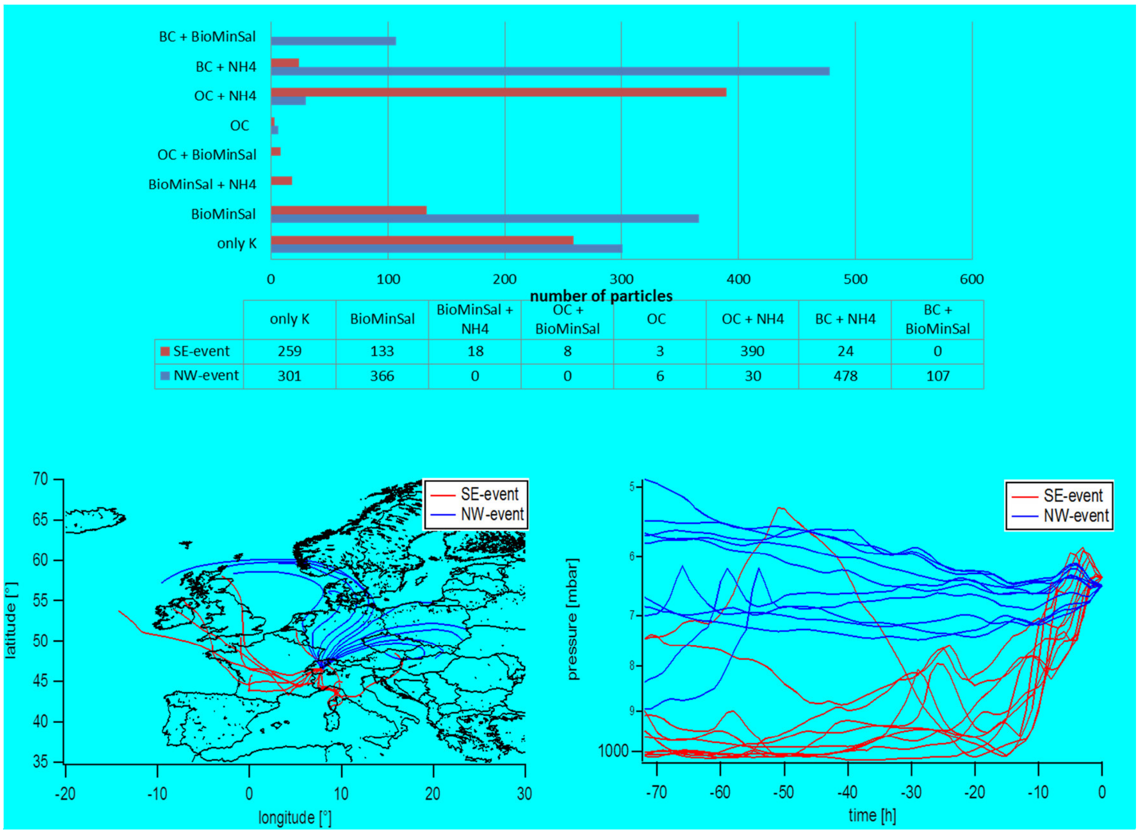

	only K	BioMinSal	BioMinSal + NH4	OC + BioMinSal	OC	OC + NH4	BC + NH4	BC + BioMinSal
🟥 SE-event	259	133	18	8	3	390	24	0
🟦 NW-event	301	366	0	0	6	30	478	107

Figure 9: Comparison of two events measured during non-cloud episodes. The northwestern event (NW; blue) was on 19.02.2013 14:00 – 16:14 and the southeastern event (SE; red) was on 11.02.2013 10:32 – 14:27. 72 h back trajectories were calculated with one trajectory every 2 hours.

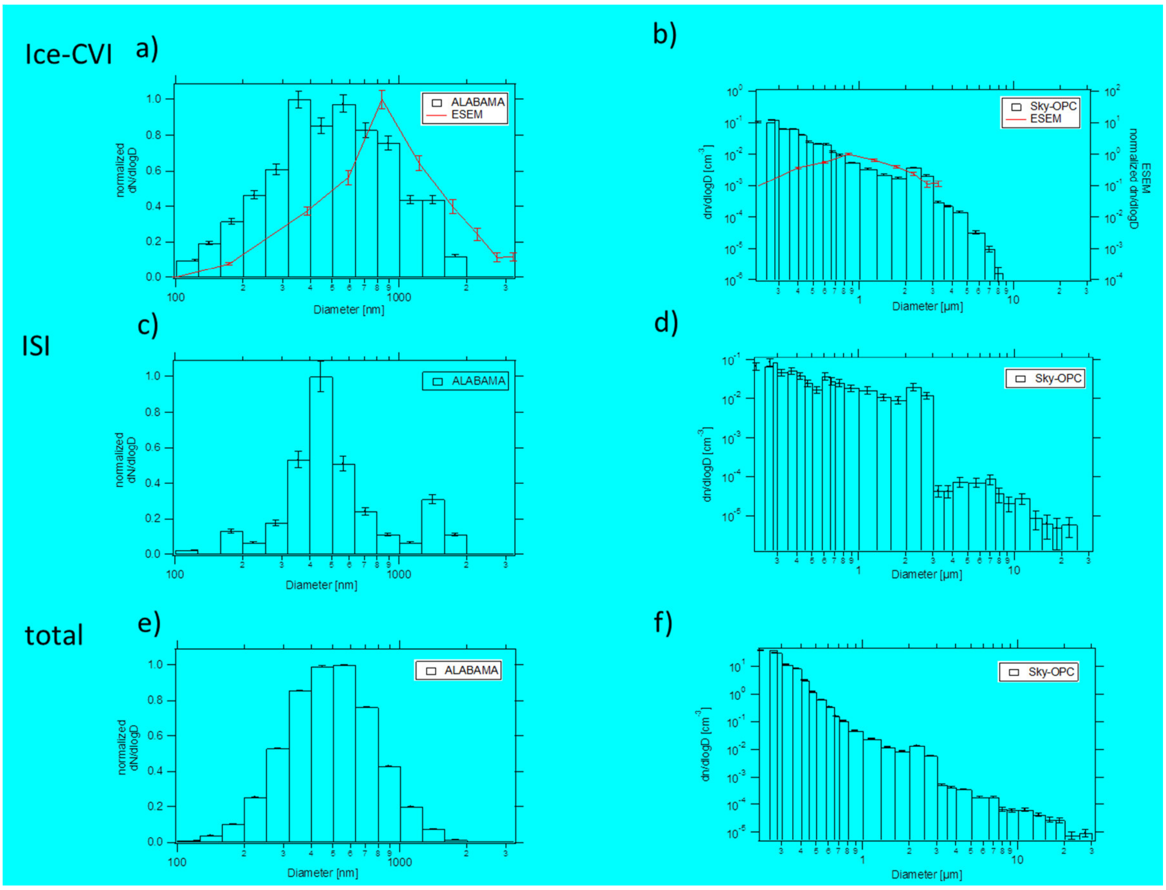

Figure 10: Measured size distribution of the IPR and background aerosol particles with the ALABAMA (bars; a, c, e) and Sky-OPC (bars; b, d, f) compared with the off-line SEM analysis of IPR samples (line; a and b). The error bars for the ALABAMA data result from counting statistics (averaged errors; $\Delta_{\text{Ice-CVI}} = 5.5\ \%$; $\Delta_{\text{ISI}} = 8.3\ \%$; $\Delta_{\text{total}} = 4\ \%$). The error of the OPC data results from Gaussian propagation of uncertainty, including counting statistics, the manufacturer-given error of the OPC of 3 %, and the error of the enrichment factor (4 % for the Ice-CVI and 20 % for the ISI). The error of the ESEM dataset was determined by counting statistics. Note the different axis scaling. The y-axis is linear in a), c), e) and logarithmic in b), d), f). The x-axis range is 100 nm – 3250 nm in a), c), e) and 200 nm – 30 µm in b), d), f).

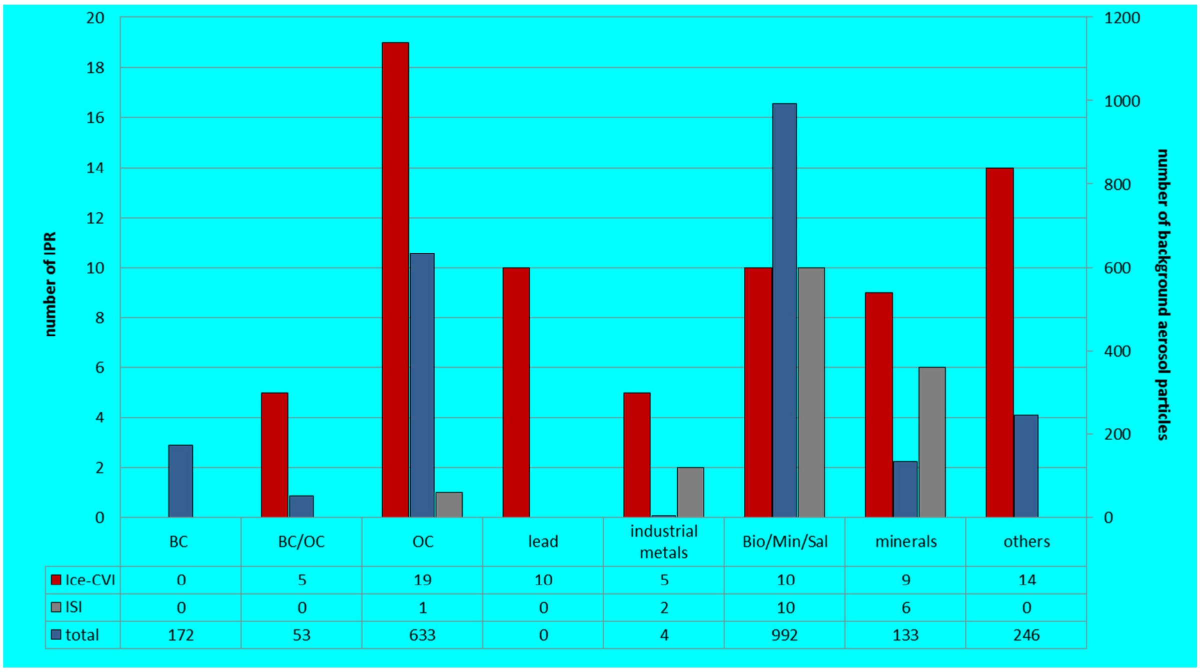

	BC	BC/OC	OC	lead	industrial metals	Bio/Min/Sal	minerals	others
🟥 Ice-CVI	0	5	19	10	5	10	9	14
■ ISI	0	0	1	0	2	10	6	0
■ total	172	53	633	0	4	992	133	246

Figure 11: Chemical composition of IPR and background aerosol particles larger than 1000 nm measured behind the Ice-CVI (red), ISI (grey) and total inlet (blue). ~~The error bars results from counting statistis.~~